Journal of Molecular Structure 1232 (2021) 129978

Contents lists available at ScienceDirect

Journal of Molecular Structure

journal homepage: www.elsevier.com/locate/molstr

Diversities in the chelation of aroylhydrazones towards cobalt(II) salts: Synthesis, spectral characterization, crystal structure and some theoretical studies

Neema Ani Mangalam[a,b], M.R. Prathapachandra Kurup[a,c,*], Eringathodi Suresh[d], Savaş Kaya[e], Goncagül Serdaroğlu[f]

[a] Department of Applied Chemistry, Cochin University of Science and Technology, Kochi, Kerala 682 022, India
[b] Department of Chemistry, Mar Thoma College, Tiruvalla, Kerala 689 103, India
[c] Department of Chemistry, School of Physical Sciences, Central University of Kerala, Tejaswini Hills, Periye, Kasaragod 671 320, Kerala, India
[d] Analytical Science Discipline, Central Salt and Marine Chemicals Research Institute, Bhavnagar 364002, Gujarat, India
[e] Sivas Cumhuriyet University, Health Services Vocational School· Department of Pharmacy, 58140, Sivas, Turkey
[f] Sivas Cumhuriyet University, Math. and Sci. Edu., 58140, Sivas, Turkey

ARTICLE INFO

Article history:
Received 29 July 2020
Revised 5 January 2021
Accepted 15 January 2021
Available online 25 January 2021

Keywords:
Aroylhydrazone
Di-2-pyridyl ketone
Crystal structure
Cobalt complex
Frontier orbital energies
Minimum polarizability

ABSTRACT

Five cobalt complexes synthesized from two aroylhydrazones were characterized by elemental analyses, thermogravimetric analysis, molar conductivity, magnetic susceptibility measurements, IR and electronic spectra. Single crystal X-ray structure of one of the complex is also reported and it got crystallized in triclinic space group $P\bar{1}$ and the crystal structure shows a distorted octahedral geometry around the metal center. Spectral data reveal that both the aroylhydrazones are tridentate and coordinate through the azomethine nitrogen, hydrazonic oxygen, and pyridyl nitrogen. Magnetic susceptibility measurements confirm the paramagnetic nature of the Co(II) complexes and one of the complex was found to be diamagnetic in nature. Additionally, HF/6-311G(d,p)/LANL2DZ calculations were performed to predict the possible intramolecular interactions contributing to the lowering of the stabilization energy. Accordingly, $\pi \rightarrow \pi^*$ transitions were found to be responsible for the stabilization energy for the ligands and their cobalt complexes. To describe and discuss the chemical reactivity and stability of synthesized complexes, quantum chemical parameters like frontier orbital energies, hardness, softness, energy gap, electronegativity, chemical potential, electrophilicity, polarizability and dipole moment were calculated. Also, the main electronic structure principles such as maximum hardness, minimum polarizability, and minimum electrophilicity principles were considered to evaluate the stability of the complexes.

1. Introduction

The architectural beauty of coordination complexes arises due to the interesting ligand systems containing different donor sites. In aroylhydrazones, it is well known that a proton transfer can occur between the hydrazinic-N and keto group of hydrazide part. Therefore, tautomerization equilibrium exists between amido form and iminol form through intramolecular proton transfer. The available donor sites in aroylhydrazone compounds are amide oxygen and azomethine nitrogen [1]. By suitable substitution on the hydrazone framework, the number of coordination sites can be increased thereby increasing the denticity. The hydrazone ligands act mostly as tridentate moieties though they have the potential to behave as bridging tetradentate ligands [2]. Among the ligand systems, hydrazide and hydrazone occupy a special place because of their straightforward synthesis, high purity and wide range of applications [3–5]. The presence of azomethine nitrogen in hydrazones is responsible for their biological importance. Metal complexes of aroylhydrazones have been studied for many years as they exhibit antimicrobial and anticancer activities [6,7]. Reported studies claim that the cadmium complex of pyridine-2-carbaldehyde isonicotinoylhydrazone could contribute alternatives as a drug candidate for the treatment of microbial diseases. Studies on cytotoxicity of cadmium complexes of hydrazones have reported that they have shown a greater effect than cis-platin [8]. It was reported recently

* Corresponding author at: Department of Applied Chemistry, Cochin University of Science and Technology, Kochi, Kerala 682 022, India.
E-mail addresses: mrp@cukerala.ac.in (M.R.P. Kurup), savaskaya@cumhuriyet.edu.tr (S. Kaya).

https://doi.org/10.1016/j.molstruc.2021.129978
0022-2860/

that judicious choice of substituents on the aromatic ring of aroylhydrazones can modulate their luminescent properties and it was also reported that on coordination with Ni(II) quenching of fluorescence has taken place [9]. This can open up the possibility of future investigations for the application of these ligands for sensing these metal ions. In addition to these, they have been studied by testing the catalytic activity of the complexes. Reports show that catalytic abilities of vanadium complexes were investigated and it was found that alcohol and/or ketone were obtained with good to excellent conversion as the main products of the hydrocarbon oxidation [10].

As a part of our studies on aroylhydrazones [3], we were eager to investigate the effect of substituents on the hydrazone framework on complexation with different metal salts. Di-2-pyridyl ketone was selected as the carbonyl part in one of the hydrazone since it can provide a further binding site for metal cation and can thus increase the denticity. The donor atoms are beautifully placed so that it provides two pockets to bind the metal ions. The choice of nicotinoylhydrazide as the hydrazide part was based on the fact that the nitrogen present in the ring can also coordinate to metal center and is capable of forming polymeric structures. This article reports the synthesis and characterization of cobalt complexes derived from some substituted aroylhydrazones. We have focused on cobalt complexes of these hydrazones as earlier reports suggest appreciable corrosion inhibiton activity and also antitumour activity [11,12]. We have also investigated the chemical reactivity, stability of the synthesized complexes, quantum chemical parameters like frontier orbital energies, hardness, softness, energy gap, electronegativity, chemical potential, electrophilicity, polarizability and dipole moment.

2. Materials and methods

2.1. Materials

Di-2-pyridyl ketone (Aldrich), 2-benzoylpyridine (Aldrich), benzhydrazide (Aldrich), and nicotinic hydrazide (Aldrich), cobalt(II) chloride dihydrate (E-Merck), cobalt(II) bromide (Aldrich), cobalt(II) acetate tetrahydrate (Nice Chemicals Pvt. Ltd.), potassium thiocyanate (Merck) and ammonium thiocyanate (E-Merck) were used as received. Solvents were purified by standard procedures before use.

2.2. Synthesis of aroylhydrazones

Aroylhydrazones were synthesized by adapting the earlier reported procedure [3], namely *via* condensation between appropriate aldehyde/ketone with the respective acid hydrazide as described below (Scheme 1).

HBPB: Selected IR (cm^{-1}) bands: ν(N–H), 3063; ν(C=O), 1678; ν(C=N), 1571.

Electronic absorption bands (MeCN) λ_{max} (nm): 233, 271, 322

HDKN: Selected IR (cm^{-1}) bands: ν(N–H), 2928; ν(C=O), 1689; ν(C=N), 1579.

Electronic absorption bands (MeCN) λ_{max} (nm): 222, 271, 321.

2.3. Syntheses of complexes

2.3.1. Syntheses of $[Co(BPB)_2]Br$ (**1**), $[Co(BPB)_2]$ (**2**), [Co(DKN)Cl] (**3**)

Complexes **1** (Scheme 2) and **3** (Scheme 3) were prepared by refluxing a corresponding methanolic solution of aroylhydrazone and cobalt salt solution in equimolar ratios after adding two drops of triethylamine for 3 h. The resulting solution was allowed to stand at room temperature and after slow evaporation; the brown-colored products were washed with ether, filtered and dried over P_4O_{10} in vacuo.

Complex **2** (Scheme 2) was prepared by a similar method using cobalt(II) acetate tetrahydrate. Dark brown crystalline product obtained washed with ether, filtered, and dried over P_4O_{10} in vacuo.

$[Co(BPB)_2]Br$ (**1**): Yield: 68%, Λ_m (DMF): 79 $ohm^{-1}cm^2\ mol^{-1}$, μ (B.M.): diamagnetic, Elemental Anal. Found (Calcd.) (%): C: 61.27 (61.72), H: 3.74 (3.82), N: 10.98 (11.36), Co: 7.43 (7.97).

$[Co(BPB)_2]$ (**2**): Yield: 73%, Λ_m (DMF): 9 $ohm^{-1}cm^2\ mol^{-1}$, μ (B.M.): 4.23, Elemental Anal. Found (Calcd.) (%): C: 68.94 (69.19), H: 4.23 (4.28), N: 12.49 (12.74), Co: 8.69 (8.93).

[Co(DKN)Cl] (**3**): Yield: 69%, Λ_m (DMF): 12 $ohm^{-1}cm^2\ mol^{-1}$, μ (B.M.): 3.95, Elemental Anal. Found (Calcd.) (%): C: 50.83 (51.21), H: 3.21 (3.54), N: 17.51 (17.56), Co: 14.39 (14.78).

2.3.2. Synthesis of [Co(BPB)NCS] (**4**) & [Co(DKN)NCS]•H_2O (**5**)

To a methanolic solution of aroylhydrazone (1 mmol), a solution of potassium thiocyanate (0.097 g, 1 mmol) in minimum volume of water was added, followed by the addition, with constant stirring, a solution of cobalt(II) acetate tetrahydrate (0.249 g, 1 mmol) in the methanol was added. The final solution was refluxed for

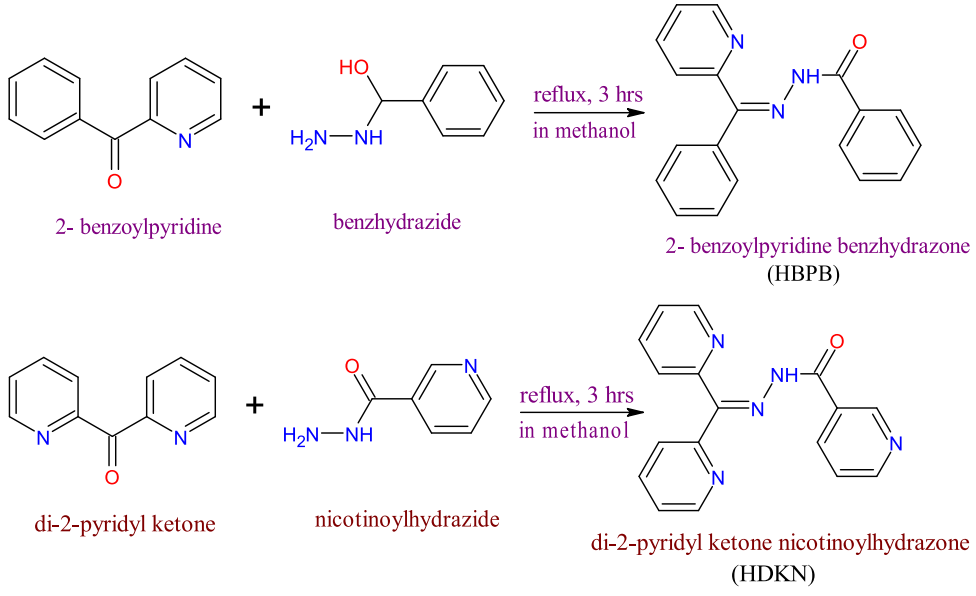

Scheme 1. Syntheses of aroylhydrazones.

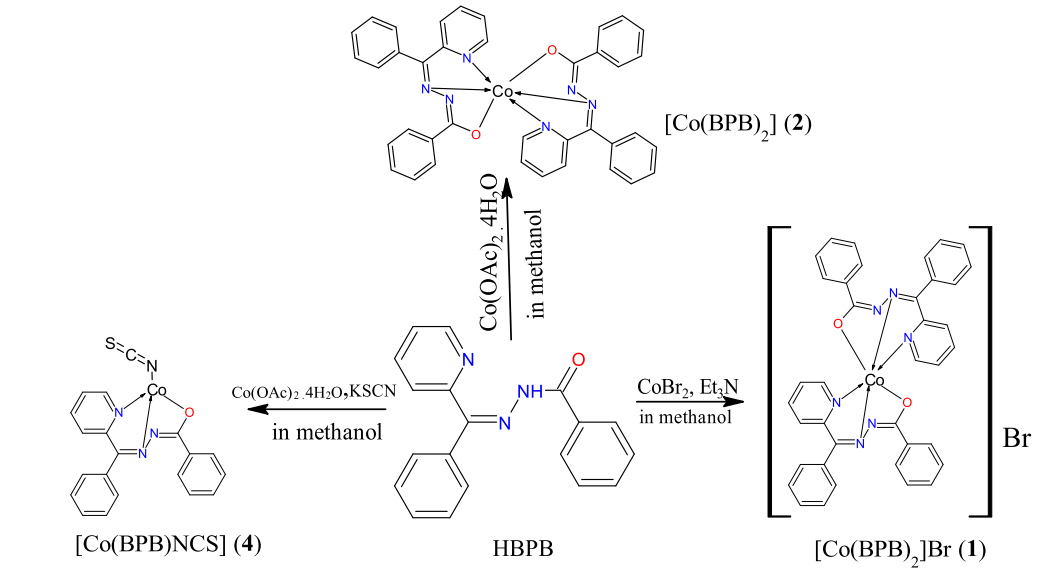

Scheme 2. Syntheses of cobalt complexes of HBPB.

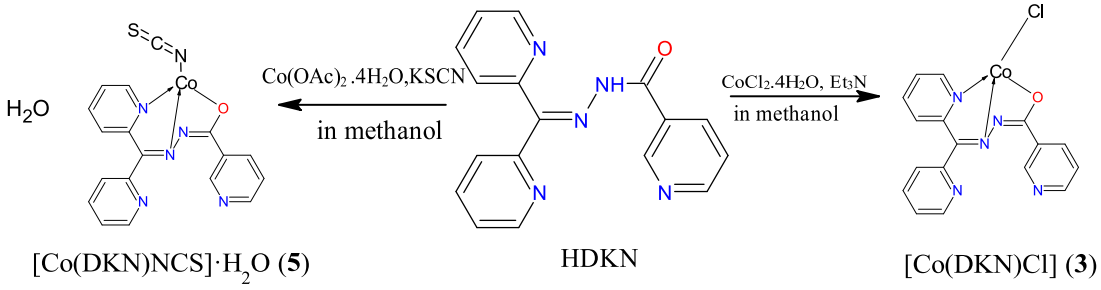

Scheme 3. Syntheses of cobalt complexes of HDKN.

3 h. and the resulting solution was allowed to stand at room temperature and after slow evaporation, the brown crystalline product was washed with ether, filtered, and dried over P_4O_{10} in vacuo (Schemes 2 and 3).

[Co(BPB)NCS] (**4**): Yield: 60%, Λ_m (DMF): 10 ohm^{-1}cm^2 mol^{-1}, μ (B.M.): 4.02, Elemental Anal. Found (Calcd.) (%): C: 57.57 (57.56), H: 3.64 (3.38), N: 13.40 (13.42), Co: 14.19 (14.12).

[Co(DKN)NCS]•H_2O (**5**): Yield: 73%, Λ_m (DMF): 5 ohm^{-1}cm^2 mol^{-1}, μ (B.M.): 4.12, Elemental Anal. Found (Calcd.) (%): C: 48.97 (49.21), H: 3.34 (3.67), N: 18.74 (19.13), Co: 13.04 (13.41).

2.4. Physical measurements

C, H and N analyses of the aroylhydrazones and the complexes were performed on a Vario EL III CHNS analyzer at SAIF, Kochi, India. The metal content of the complexes was determined by AAS after digestion with con. HNO_3. The analysis was done using Thermo Electron Corporation, M series Atomic Absorption Spectrophotometer. The IR spectra were recorded on a JASCO FT/IR-4100 Fourier Transform Infrared spectrometer using KBr pellets in the range 400–4000 cm^{-1}. Electronic spectra in acetonitrile solutions were recorded on a Spectro UV–vis Double Beam UVD-3500 spectrometer in the 200–900 nm range. ^{1}H NMR spectra of the synthesized hydrazones were recorded in $CHCl_3$-d_6 as solvent on a Bruker Avance DPX-300 MHz NMR spectrometer at NIIST, Trivandrum. Chemical shifts are reported in δ(ppm) relative to TMS as the internal standard. The molar conductance of the complexes in DMF (10^{-3} M) solutions was measured at 298 K with a Systronic model 303 direct-reading conductivity bridge. The magnetic susceptibility measurements were performed on powdered samples at 298 K using a Sherwood Scientific Magnetic Susceptibility Balance (M.S.B) MK1 using $HgCo(SCN)_4$ as calibrant, the diamagnetic contribution to the susceptibility was estimated through Pascal's constants.

2.5. X-ray crystallography

A plate-like brown crystal of [Co(BPB)$_2$] with dimensions 0.32 × 0.22 × 0.20 mm^3 was selected and diffraction data was collected on a Bruker SMART APEX diffractometer equipped with graphite monochromated radiation (λ = 0.71073 Å) by using the φ/w scan technique at room temperature. The structure was solved by direct methods and refined by full-matrix least-squares on F^2 using the SHELXL-2018/3 [13] program package. All non-hydrogen atoms were subjected to anisotropic refinement and all the hydrogen atoms were assigned with common isotropic displacement factors and were included in the final refinement by use of geometrical constraints.

Crystal data and details of the refinement for [Co(BPB)$_2$] (**2**) are summarized in Table 1 and selected bond lengths (Å) and angles (°) are presented in Table 2. The molecular structure of complex **2** showing the atom labeling scheme and the remaining crystallographic figures showing the intermolecular forces (Fig. 2) and packing (Fig. 3) were drawn using DIAMOND version 3.2 g [14].

2.6. Computational details

Ab initio calculations of the ligands (HBPB and HDKN) and five complexes were performed by G09W package [15] at HF/6-311G(d,p)/LANL2DZ [16] in the gas phase. After the geometry op-

Table 1
Crystal data and structure refinement parameters for complex **2**.

Parameters	$[Co(BPB)_2]$ (**2**)
Empirical Formula	$C_{38}H_{28}CoN_6O_2$
Formula weight (M)	659.59
Temperature (T) K	273(2)
Wavelength (Mo Kα) (Å)	0.71073
Crystal system	Triclinic
Space group	$P\bar{1}$
Lattice constants a (Å), b (Å), c (Å), α (°), β (°). γ (°)	10.728(2), 2.498(3), 12.883(3), 66.802(3), 83.614(4), 83.103(4)
Volume V (Å^3)	1572.3(6)
Z Calculated density (ρ) (Mg m^{-3})	2 1.393
Absorption coefficient, μ (mm^{-1})	0.591
Limiting Indices	$-13 \leq h \leq 13$, $-15 \leq k \leq 15$, $-15 \leq l \leq 15$
Reflections collected	10,982
Unique Reflections	6181 [R(int) = 0.0386]
Refinement method	Full-matrix least-squares on F^2
Data / restraints / parameters	6182 / 0 / 424
Goodness-of-fit on F^2	1.010
Final R indices [I > 2σ (I)]	$R_1 = 0.0824$, $wR_2 = 0.1925$
R indices (all data)	$R_1 = 0.1134$, $wR_2 = 0.2289$

$R_1 = \Sigma||F_o| - |F_c|| / \Sigma|F_o|$, $wR_2 = [\Sigma w(F_o^2-F_c^2)^2 / \Sigma w(F_o^2)^2]^{1/2}$.

Table 2
Selected bond lengths (Å) and bond angles (°) for $[Co(BPB)_2]$

Bond lengths		Bond angles	
Co1–N2	2.0364(4)	N2–Co1–N5	169.89(18)
Co1–N5	2.0264(4)	N2–Co1–O1	76.34(17)
Co1–O1	2.054(4)	N2–Co1–N1	77.00(17)
Co1–O2	2.092(3)	N5–Co1–O2	75.73(15)
Co1–N1	2.139(5)	N5–Co1–N4	76.35(17)
Co1–N4	2.151(4)	O1–Co1–N1	153.20(16)
N2–N3	1.360(6)	O2–Co1–N4	151.08(16)
N5–N6	1.368(5)	N5–Co1–N1	94.04(17)
N2–C6	1.296(7)	N2–Co1–N4	99.83(17)
N5–C25	1.294(6)	N1–Co1–N4	96.84(17)
O1–C13	1.286(6)	N4–Co1–O1	90.38(17)
O2–C32	1.266(6)	N1–Co1–O2	92.49(17)
N3–C13	1.343(7)	N2–Co1–O2	108.94(16)
N6–C32	1.346(6)	O2–Co1–O1	93.52(16)
C13–C14	1.488(8)	C6–N2–N3	122.1(4)
C32–C33	1.495(7)	C25–N5–N6	120.4(4)

timizations of all molecules and verifying these structures, NBO analysis [17,18] was conducted to estimate the possible intramolecular interactions. Frontier molecular orbital investigations [19–21] were employed to evaluate/ compare the reactivity behavior.

In the Conceptual Density Functional Theory known as Density Functional Theory of chemical reactivity, chemical reactivity descriptors like hardness (η), electronegativity (χ), softness (σ) and chemical potential (μ) are given as the derivatives concerning the number of electrons (N) and the total electronic energy (E) at a constant external potential. The equations based on ionization energy (I) and electron affinity (A) parameters of the descriptors have been obtained by Pearson and Parr with the help of the finite differences approach [22].

$$\mu = -\chi = \left[\frac{\partial E}{\partial N}\right]_{v(r)} = -\left(\frac{I+A}{2}\right)$$

$$\eta = \frac{1}{2}\left[\frac{\partial^2 E}{\partial N^2}\right]_{v(r)} = \frac{I-A}{2}$$

$$\sigma = 1/\eta$$

As is known, Molecular Orbital Theory explains the reactivity of molecules *via* frontier orbital energies. Using Koopmans Theorem, ionization energy and electron affinity values of molecules can be approximately predicted. In the mentioned theory, it is accepted that negative values of HOMO and LUMO orbital energies of any molecule correspond to ionization energy and electron affinity values of the molecule. In the framework of this information, the following mathematical expressions can be written [23].

$$I = -E_{HOMO}$$

$$A = -E_{LUMO}$$

Electrophilic powers of molecules are associated with their chemical hardness and electronegativity (or chemical potential) values through electrophilicity index (ω) which was introduced by Parr, Liu, and Szentpaly [24]. After the electrophilicity index was imparted to science, Chattaraj [25] defined nucleophilicity (ε) as the multiplicative inverse of the electrophilicity index. These definitions proposed by said scientists are widely used in the studies regarding organic reaction mechanisms.

$$\omega = \chi^2/2\eta = \mu^2/2\eta$$

$$\varepsilon = 1/\omega$$

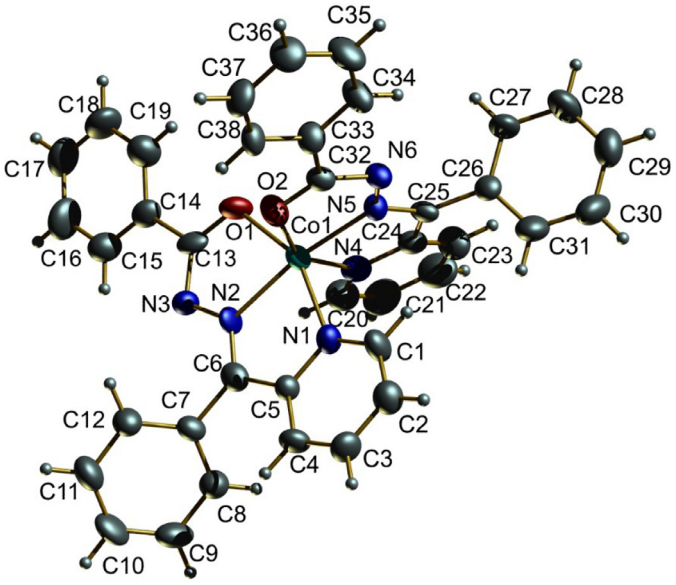

Fig. 1. The molecular structure of $[Co(BPB)_2]$ (**2**) along with the atom numbering scheme.

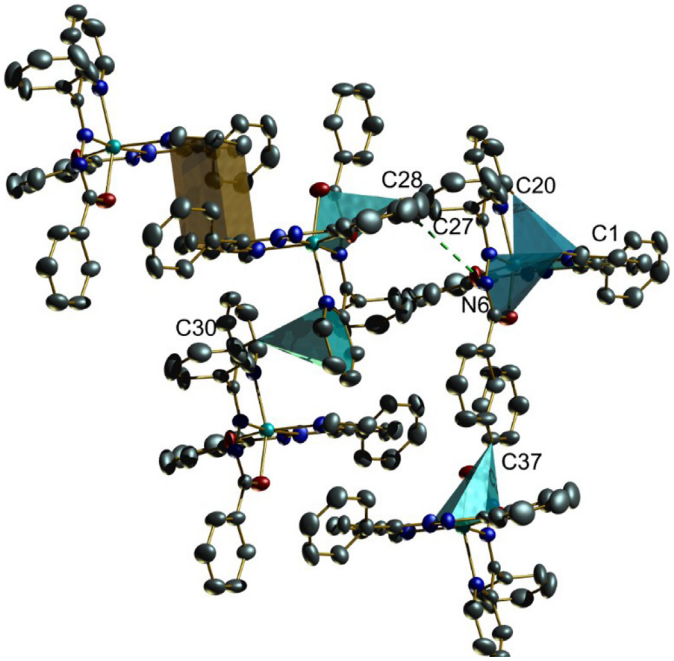

Fig. 2. Intermolecular forces in $[Co(BPB)_2]$.

One of the parameters providing information about electron-donating ability, electron-accepting ability, and stability of chemical compounds is polarizability (α). There is a remarkable correlation between polarizability and softness. This parameter is calculated depending on diagonal components of polarizability tensor *via* the following equation.

$$\langle\alpha\rangle = 1/3[\alpha_{xx} + \alpha_{yy} + \alpha_{zz}]$$

Also, HOMO & LUMO and MEP plots were visualized by Gaussview 6.01 package [26] to show the nucleophilic and electrophilic attack sites.

3. Results and discussion

3.1. NMR spectra of aroylhydrazones

The ^{1}H NMR spectra of HBPB and HDKN were recorded in $CDCl_3$ and are shown in Fig. S1. The sharp signals at δ = 15.2 and δ = 15.7 ppm are due to the existence of the ligands in iminol form in $CDCl_3$. On D_2O exchange the intensity of this signal is found to be considerably decreased. Aromatic protons appear as multiplets at 7.2–8.8 ppm range.

3.2. Crystal structure of $[Co(BPB)_2]$ (**2**)

Brown plate-shaped crystals of **2** were obtained by slow evaporation from a mixture of dichloromethane-methanol (1:1 v/v) solution of $[Co(BPB)_2]$. The molecular structure of $[Co(BPB)_2]$ along with the atom numbering scheme is depicted in Fig. 1. The bond distances and angles (Tables 1 and 2) reveal that the independent units of the molecule exist in a distorted octahedral geometry around the metal center. Here we can see that the Co(II) center is coordinated by each of the hydrazone moiety through *cis* pyridyl nitrogen, trans azomethine nitrogen and *cis* enolate oxygen atoms in an N_4O_2 meridional manner [27,28]. The higher strength of Co–N_{azo} compared to Co–N_{py} bond is evident from their bond lengths. This observation is also seen in Mn complexes of similar ligands [29], but this is little bit different in copper(II) complexes of hydrazones, where one of the pyridyl nitrogen and enolate oxygen are slightly longer than the remaining four bond lengths [30]. On complexation, we can see that the carbonyl bond distance is increased when compared to the corresponding value in the free ligand 1.2213(14) Å [3], and this supports coordination through enolate oxygen. A delocalized conjugating effect along the metal-chelate rings is generated by a significant amount of metal-to-ligand π back bonding and this imparts partial single and double bond nature to the C6–N2 and N2–N3 hydrazine bonds in the hydrazone moiety owing to the extensive delocalization over the entire coordination framework [31].

Four fused five-membered chelate rings share the metal center. The dihedral angle between the planes constituting Co1, N1, C5, C6, N2 and Co1, N2, N3, C13, O1 with a maximum deviation from the mean plane of 0.0528 Å for C5 and 0.0571 Å for N2 respectively is found to be 3.47°. The trans angle N2–Co1–N5 is much farther from 180° compared to Cu(II) complexes reported with HBPB hydrazone [32]. It is found that this deviation is highest for Mn(II) complexes of similar hydrazones [33]. The intraligand bite angles also become more acute (75.73°−77.00°) in this complex when compared to its Cu(II) complex, but this was more pronounced in the Mn(II) complex (70.85°−72.41°). The two ligand moieties in the present compound are aligned almost perpendicular to each other as revealed from the dihedral angle of 87.95° between the plane containing atoms {N1, C5, C6, N2, N3, C13, O1, Co1} with that to second plane {N4, C24, C25, N5, N6, C32, O2, Co1}.

There are no classic hydrogen bonds seen in the crystal structure. However, some weak hydrogen bonding and C–H•••π interactions including that between metal-containing chelate ring Cg(2) with the protons on C(28), Cg(6) with protons on C(30) and chelate ring Cg(1) with protons on C(37) [34] are seen in the crystal lattice (Fig 2, Table 3). There is also a π-π interaction between the pyridyl ring of a molecule with the pyridyl ring of another molecule with a distance of 3.81 Å (Fig. 2). The orientation in the close packing (Fig. 3) is in such a way that molecules are interconnected through these interactions.

3.3. Molar conductivity and magnetic susceptibility measurements

The molar conductance value of $[Co(BPB)_2]Br$ was found to be 79 ohm^{-1} cm^2 mol^{-1} showing that it is a 1:1 electrolyte,

Table 3
H-bonding, π-π and C–H•••π interaction parameters of [Co(BPB)$_2$] (**2**).

H-bonding Donor•••H•••A (Å)	D–H	H•••A	D•••A	D–H•••A
C27–H(27)•••N(6)[a]	0.93	2.56	3.3207	139
π-π interactions				
Cg(I) •••Cg(J)	Cg–Cg (Å)	α (°)	β (°)	
Cg(5)•••Cg(5)[b]	3.8100	0.00	22.45	
C–H•••π interaction				
X–H(I)•••Cg(J)	H•••Cg (Å)	X–H•••Cg (°)	X•••Cg (Å)	
C(28)–H(28) •••Cg(2)[c]	2.80	138	3.5389	
C(30)–H(30) •••Cg(6)[d]	2.95	141	3.7133	
C(37)–H(37) •••Cg(1)[e]	2.99	137	3.7158	
Equivalent position codes				
a = 1-x,1-y,1-z,	b = 2-x,-y,1-z,	c = 1-x,1-y,1-z,	d = 2-x,1-y,1-z	e = 1-x,-y,1-z

D, donor; A, acceptor; Cg, centroid; α (°) = Dihedral angle between planes I and J
β (°) = Angle between Cg(I)–Cg(J) vector and Cg(J) perp

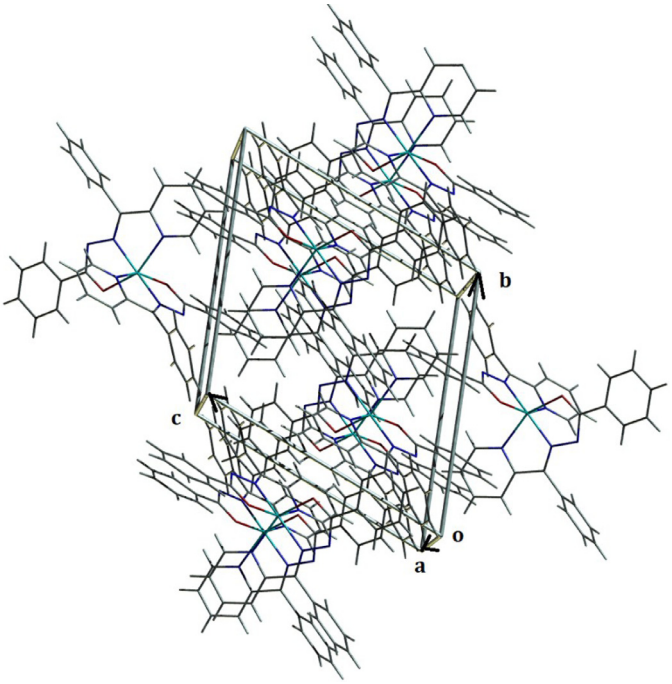

Fig. 3. Packing diagram of [Co(BPB)$_2$] (**2**).

while others have very low values in the range 4–12 ohm^{-1} cm^2 mol^{-1} indicating their non-electrolytic nature [35]. The complex [Co(BPB)$_2$]Br was found to be diamagnetic in nature, which illustrates that it has no unpaired electrons. Here the metal is in +3 oxidation state with a spin paired octahedral configuration. The observed magnetic moment for the octahedral complex [Co(BPB)$_2$] is found to be 4.23 B.M. which is higher than calculated by the spin-only formula [36]. This suggests that there is an orbital contribution. In octahedral complexes, Co^{2+} has $(t_{2g})^5(e_g)^2$ configuration and is possible to transform an orbital into an equivalent (degenerate) orbital by rotation. This suggests that complex **2** has a high spin octahedral configuration. The magnetic moment of the other three complexes is found in 3.95–4.12 B.M. range suggesting a tetrahedral geometry [37].

3.4. Infrared spectra

The significant IR frequencies of the ligands are given in the experimental section. The IR spectra of ligands (Fig. S2) showed strong bands at ~3000 and ~1680 cm^{-1} which are assigned to ν(N–H) and ν(C=O) vibrations, respectively, suggesting that the hydrazones are present in the amido form in solid state [38]. Spectral assignments of the complexes made are compared with that of the hydrazones and are tabulated in Table 4. In all the complexes there are no characteristic bands of amide and amino groups suggesting that both the hydrazones are coordinated to the metal center in the enolate form [39]. However a new band at ~1370 cm^{-1} is observed which is ascribed to ν(C–O) stretching suggesting the enolisation of –C=O of acyl keto group giving rise to –C=N–C=N- moiety [40]. In addition to this, the band corresponding to the azomethine stretching shows a downward shift indicating that the nitrogen of the azomethine group is ligated to the metal center [41]. A new band at ~ 1590 cm^{-1} is observed which may be due to the new ν(C=N) band which supports the participation of azomethine nitrogen in coordination [42]. The pyridyl in-plane ring deformation and out-of-plane ring deformation are found at higher frequencies compared to that of the ligands suggesting the coordination of pyridyl nitrogen [43].

The IR pattern of thiocyanato complexes is similar to that of the other complexes discussed above and the major difference lies in the 2100–2000 cm^{-1} region of the spectrum. The most interesting peaks in the IR spectra of these complexes is a sharp band at 2062 cm^{-1} in [Co(BPB)NCS] and 2070 cm^{-1} in [Co(DKN)NCS]•H_2O [44]. The position of peak and its structure (singlet) points out to the presence of N-bonded terminal thiocyanate group in the complex. The ν(CS) of NCS ligand at 774 and 758 cm^{-1} indicates the coordination through nitrogen atom of terminal NCS ligand [5,45] but the bending vibration of NCS group which is expected near 480 cm^{-1} are normally weak and tend to be obscured by other bands. For complex **5**, a broad band due to the presence of lattice water in the complex was seen at 3420 cm^{-1} which was also evident from the thermogravimetric analysis. The TGA curve for complex **5** displayed the first stage of decomposition in the range 60–110 °C, which is due to the loss of one molecule of water with 3.90% of the total weight of the complex (Calcd. 4.09%) (Fig. 4).

3.5. Electronic spectra

The electronic spectra of aroylhydrazones and the complexes (10^{-5} M) were recorded in acetonitrile solution and spectral data are summarized in Table 5. The n→π^* and π→π^* transitions of the uncomplexed hydrazones are slightly shifted upon complexation. The bands in the range of 384 - 410 nm correspond to the ligand to metal charge transfer (LMCT) transitions [46] (Fig. 5).

The terms arising for a Co^{2+} (d^7 system) are the ground state ^{3}F and the excited states ^{3}P, ^{1}G, ^{1}D, ^{1}S. The transitions from the ground state to the three singlet states (^{1}G, ^{1}D, ^{1}S) are spin forbidden and will be very weak and can be ignored. The two remaining states ^{3}F and ^{3}P can have spin permitted transitions. The F state split into A_{2g}+T_{1g}+T_{2g} and P state is transformed into a

Table 4
Infrared spectral assignments (cm^{-1}) of the cobalt complexes.

Compound	ν(C–O)	ν(C=N)	ν(C=N)[a]	ν(Co–O)	ν(Co–N)
$[Co(BPB)_2]Br$ (**1**)	1368	1558	1595	531	475
$[Co(BPB)_2]$ (**2**)	1360	1541	1584	535	445
[Co(DKN)Cl] (**3**)	1377	1508	1589	548	470
[Co(BPB)NCS] (**4**)	1373	1551	1597	538	479
$[Co(DKN)NCS]\bullet H_2O$ (**5**)	1364	1509	1584	550	470

[a] Newly formed C=N.

Table 5
Electronic spectral data of the cobalt(II//III) complexes.

Compound	Intaligand transitions		LMCT		d-d transitions	
	λ_{max} (nm)	ε ($M^{-1}cm^{-1}$)	λ_{max} (nm)	ε ($M^{-1}cm^{-1}$)	λ_{max} (nm)	ε ($M^{-1}cm^{-1}$)
HBPB	233 271 322	5.25×10^3, 4.488×10^3, 5.164×10^3	–-	–-	–-	–-
HDKN	222 271 321	5.038×10^4, 4.855×10^4, 5.174×10^4	–-	–-	–-	–-
$[Co(BPB)_2]Br$ (**1**)	222 288	7.35×10^4, 4.56×10^4	408	2.854×10^4	549	5.7×10^2
$[Co(BPB)_2]$ (**2**)	258 282	3.015×10^4, 2.536×10^4	384	2.457×10^4	551	5.61×10^2
[Co(DKN)Cl] (**3**)	224 246 285	5.44×10^3, 4.489×10^3, 4.079×10^3	407	2.387×10^3	590, 666	5.43×10^2, 3.67×10^2
[Co(BPB)NCS] (**4**)	230 290	2.97×10^4, 2.05×10^4	410	1.18×10^4	588, 625	2.17×10^3, 3.73×10^3
$[Co(DKN)NCS]\bullet H_2O$ (**5**)	222 285	7.367×10^3, 4.763×10^3,	403	2.615×10^3	585, 619	3.53×10^3, 4.21×10^3

T_{1g} state. Hence three peaks should appear in the spectrum corresponding to $^4T_{2g}(F) \leftarrow {}^4T_{1g}(F)$, $^4A_{2g}(F) \leftarrow {}^4T_{1g}(F)$ and $^4T_{1g}(P) \leftarrow {}^4T_{1g}(F)$. There are two T_{1g} states and since they are of the same symmetry, they interact with one another and this interelectronic repulsion is much more marked in d^7 T_d case. Due to this, they may cross each other but it is impossible because states of the same symmetry cannot cross each other. But this occurs in O_h case and thus $^4A_{2g} \leftarrow {}^4T_{2g}$ transition is very weak.

In tetrahedral complexes of $Co^{2+}$the electronic arrangement is $(e)^4(t_2)^3$. Three transitions are expected, $^4T_2(F) \leftarrow {}^4A_2$, $^4T_1(F) \leftarrow {}^4A_2$, $^4T_1(P) \leftarrow {}^4A_2$. In the Co(II) complexes except $[Co(BPB)_2]$, two bands in the range 585 - 666 nm are observed corresponding to $^4T_1(F) \leftarrow {}^4A_2$ and $^4T_1(P) \leftarrow {}^4A_2$ transitions [47,48] (Fig. 6), but the other transition lies in the near IR region and is not observed as it is out of the range of the used spectrophotometer (200–900 nm). In complex $[Co(BPB)_2]$, a weak band at 551 nm was found which can be assigned to $^4T_{1g}(P) \leftarrow {}^4T_{1g}(F)$ transition [11,31]. In the case of $[Co(BPB)_2]Br$, cobalt is in +3 oxidation state with a d^6 electronic configuration. So only one weak d-d transition is observed at 549 nm. These values were in agreement with reported octahedral cobalt complexes [49,50]

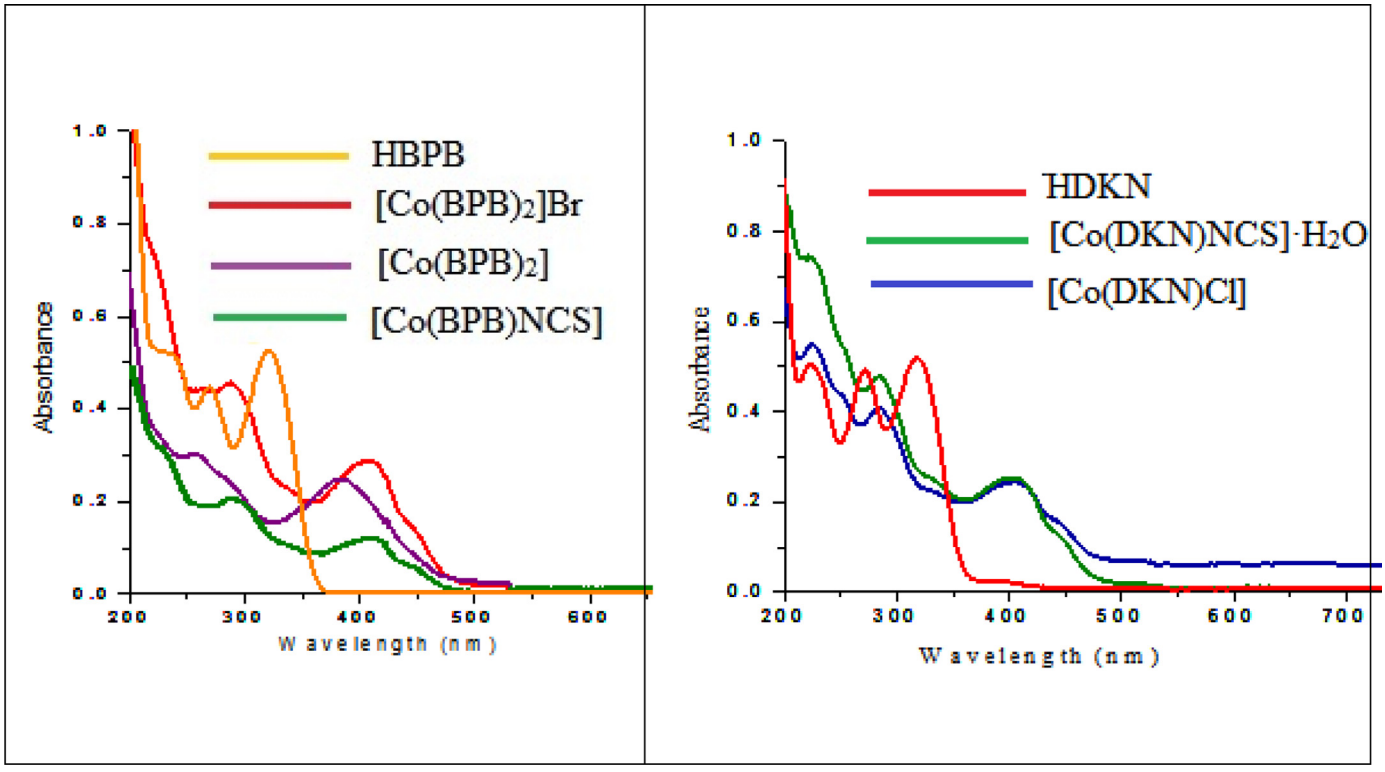

Fig. 5. Electronic spectra of the Co(II/III) complexes in the region 200–700 nm.

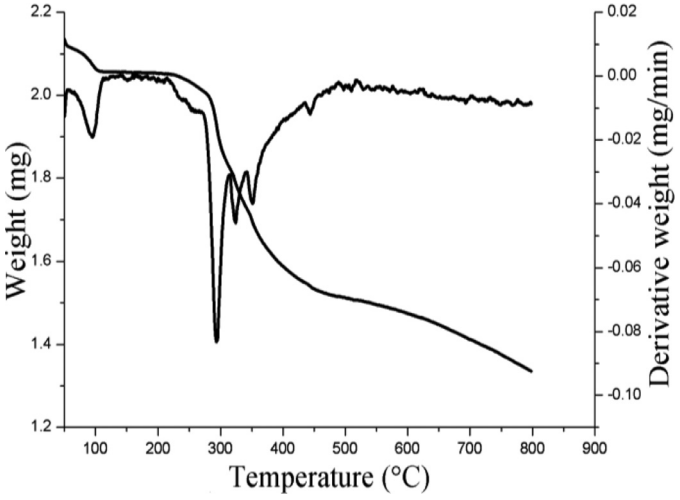

Fig. 4. TG-DTG curve of [Co(DKN)NCS]•H_2O (**5**).

3.6. Natural bond orbitals

The NBOs for the ligands and their cobalt complexes are analyzed to predict the possible intramolecular interactions, and the results are given in Tables S1 and S2 (supl. data). The optimized geometries along with atom labeling of the ligands and complexes are presented in Fig. 7. From Table S1, the highest contribution to the stabilization energy ($E^{(2)}$) of each ligand are sourced from the $\pi \rightarrow \pi^*$ resonance interactions: $E^{(2)}$ for π C32-C38$\rightarrow \pi^*$ C26-C28 (HBPB) and π C26-C27$\rightarrow \pi^*$ C28-N35 (HDKN) interactions are 46.31 and 33.19 kcal/mol, respectively. It is also found from Table S1 that the resonance energy for the C1-N11$\rightarrow \pi^*$ C2-N12 and C2-N12$\rightarrow \pi^*$ C3-C4 interactions are 8.75 and 23.53 kcal/mol for HBPB proligand, and 4.09 and 11.67 kcal/mol for HDKN ligand, respectively. It is worth to mention that the count of the resonance interactions for HDKN proligand is greater than that of the HBPB proligand because of the nicotinoyl hydrazide moiety. For instance, HDKN has additionally the C14-N36$\rightarrow \pi^*$ C15-C16 (11.73 kcal/mol), C14-N36$\rightarrow \pi^*$ C18-C19 (25.84 kcal/mol), the C28-N35$\rightarrow \pi^*$ C26-C27 (12.22 kcal/mol), and the C28-N35$\rightarrow \pi^*$ C29-C32 (29.65 kcal/mol) interactions over this nicotinoyl hydrazide moiety. One remarkable n$\rightarrow\pi^*$ interaction is calculated for both ligands: the stabilization energy of LP (1) N13$\rightarrow \pi^*$ C1-N11 and LP (1) N13$\rightarrow \pi^*$ C23-O25 interactions are determined as 18.65 and 32.83 kcal/mol for HDKN and, 39.80 and 70.18 kcal/mol for HBPB.

On the other hand, the chelation of the HBPB and HDKN towards the cobalt center affects the donor-acceptor interactions, more or less according to the substituent group on the complexes. For complexes **1** and **2** synthesized by using the HBPB ligand, the stabilization energy for the interaction of the lone pair of the nitrogen atom to cobalt is calculated as 8.42- 34.42 kcal/mol and 6.78–35.16 kcal/mol, respectively. Besides, the charge transfer from the lone pair of oxygen atoms to cobalt contributed to the stabilization of complexes **1** and **2** are calculated as 5.26- 43.13 kcal/mol for complex **1** and as 5.24–43.37 kcal/mol for complex **2**, respectively. Also, the electron delocalization energies of the LP (3) O16$\rightarrow$ LP*Co (EDi=0.83778e) and LP (3) O32$\rightarrow$ LP*Co (EDi=0.83786e) interactions for complex **2**, are the highest contributed interactions, are calculated at 43.31 and 43.37 kcal/mol. The other highest energy interactions for complex **1** is due to the electron delocalization over the main body of the complex, which are π C4-C7$\rightarrow \pi^*$ C6-N12 and π C20-C23$\rightarrow \pi^*$ C22-N28 with the $E^{(2)}$=38.41 kcal/mol (EDi=0.80860e) and $E^{(2)}$=38.00 kcal/mol (EDi=0.80901e), respectively. Also, the electron moving from the Cl atom towards Co(II) atom contributes to stabilizing complex **3** with the energy of 9.89 and 6.50 kcal/mol. On the other hand, the highest contribution to the stabilization energy of complex **3**, except for the resonance interactions, is sourced from the charge movement to Co(II) atom from the lone pair of O atom on the main skeleton of the complex, with the energy of 13.28 kcal/mol. For the complexes **4** and **5** including the -N=C=S fragment, the resonance energy for LP (2) S$\rightarrow \pi^*$ N30-C31 and LP (2) S$\rightarrow \pi^*$ N39-C40 are calculated as 58.73 and 93.59 kcal/mol, which are the highest contribution to the stabilization of these complexes.

3.7. Frontier molecular orbitals and chemical reactivity

As given above, frontier orbital energies are widely considered in the reactivity analysis of molecules. In this context, Koopmans Theorem can be considered as a bridge between Molecular Orbital Theory and Conceptual Density Functional Theory. The quantum chemical descriptors for the two proligands and the complexes were calculated and are given in Table 6. Electronic structure principles known as maximum hardness principle [51], minimum polarizability principle [52] and minimum electrophilicity principle [53] provide great amenities to chemists in terms of the prediction of the stability of molecules and directions of chemical reactions. Pearson defined the chemical hardness as the resistance towards electron cloud polarization or deformation of chemical species and proposed two reactivity principles about this concept [54]. One of them is Maximum hardness principle which states that “there seems to be a rule of nature that molecules arrange themselves to be as hard as possible.” This means that chemical hardness is a measure of stability and hard molecules are more stable compared to soft ones. It is apparent from the hardness data given in the related table that complex **2** is more stable compared to others. According to the Minimum electrophilicity principle introduced by Chattaraj [25], in a stable state, electrophilicity is minimized. If so, the complex having the lowest electrophilicity index value should be more stable. This principle also supports the idea that the most stable one among the studied complexes is complex **2**. The results obtained in the light of maximum hardness and minimum electrophilicity principles are compatible with each other. Molecules with high polarizability and dipole moment are quite reactive. The validity of this information is supported via the minimum polarizability principle. Although complex **1** has a high polarizability value, the dipole moment value of complex **2** is lower compared to others. If so, one can say that almost all electronic structure principles point to the same complex as the most stable complex.

The chemical reactive sites for the proligands and cobalt complexes are presented in Fig. 8 by visualizing HOMO, LUMO, and MEP plots. Accordingly, the HOMO for the HDKN and HBPB ligands concentrates on the whole surface except for the phenyl- and pyridine- rings, respectively. On the other hand, LUMO density for both proligands expanded over the whole molecular surface. For all the complexes, the chelation of each ligand to the metal makes the nucleophilic attack center shifted to the metal center (electron-poor region). In this context, there is no HOMO density on the phenyl- rings for **1, 2**, and **4** complexes, on the pyridine- ring(s) for **3** and **5** complexes. One of the remarkable results of these plots is that the LUMO for complexes **1** (except for the bromine ion) and **2** expands over the whole molecular surface while the LUMO density for the other complexes expands around the metal center and of the substituent atom (or groups). For instance, the LUMO for **4** and **5** complexes is quite distributed on the substituted -NCS part and over Co(II). Also, it can be said that all compounds are more enthusiastic against nucleophilic attacks than the electrophilic attacks because of the dominant blue color over the molecular surfaces of the complexes while the ligands present two possible regions for both the nucleophilic (blue) and electrophilic attacks (red).

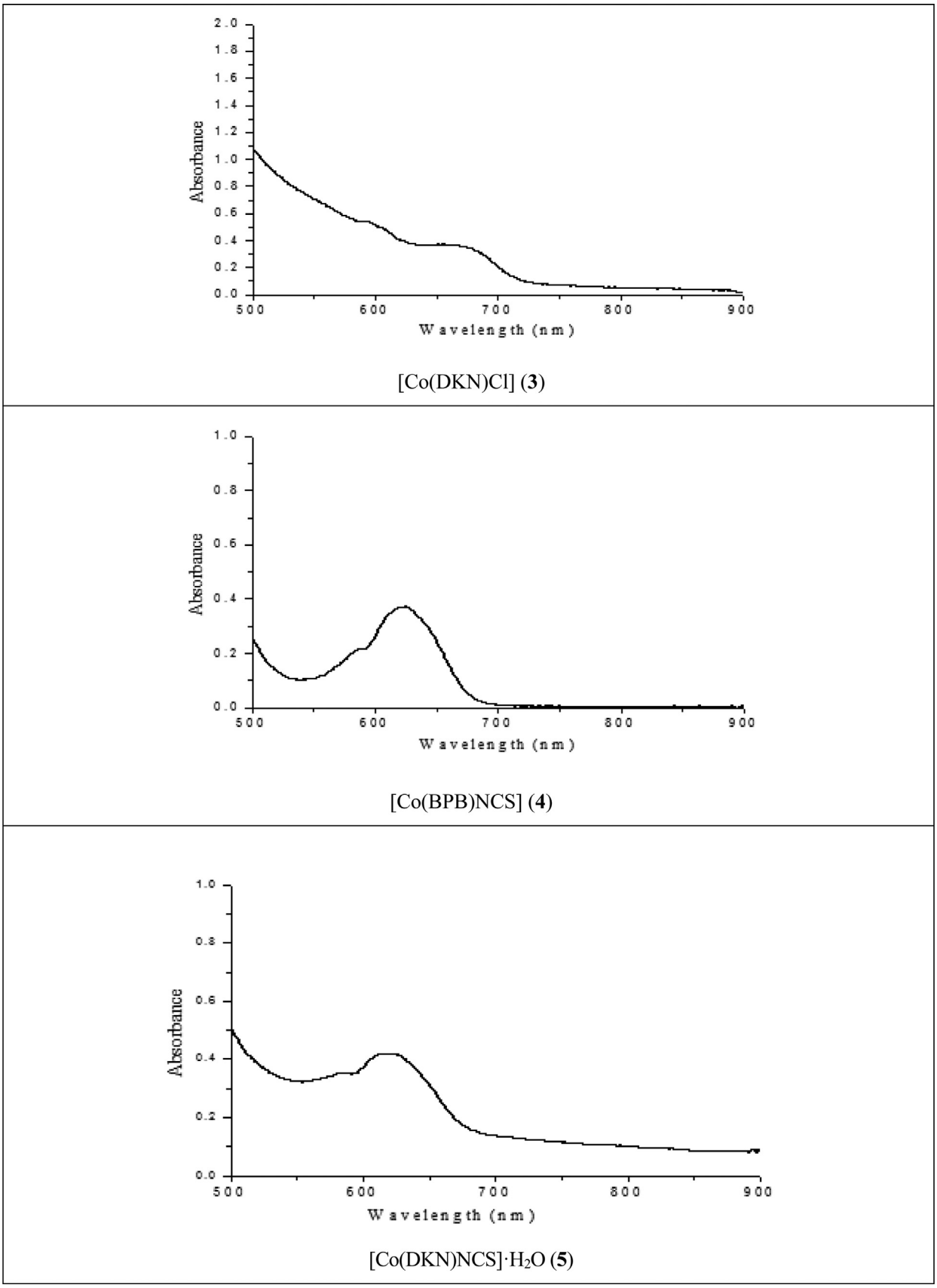

Fig. 6. Electronic spectra of complexes **3, 4** & **5** in the region 500–900 nm.

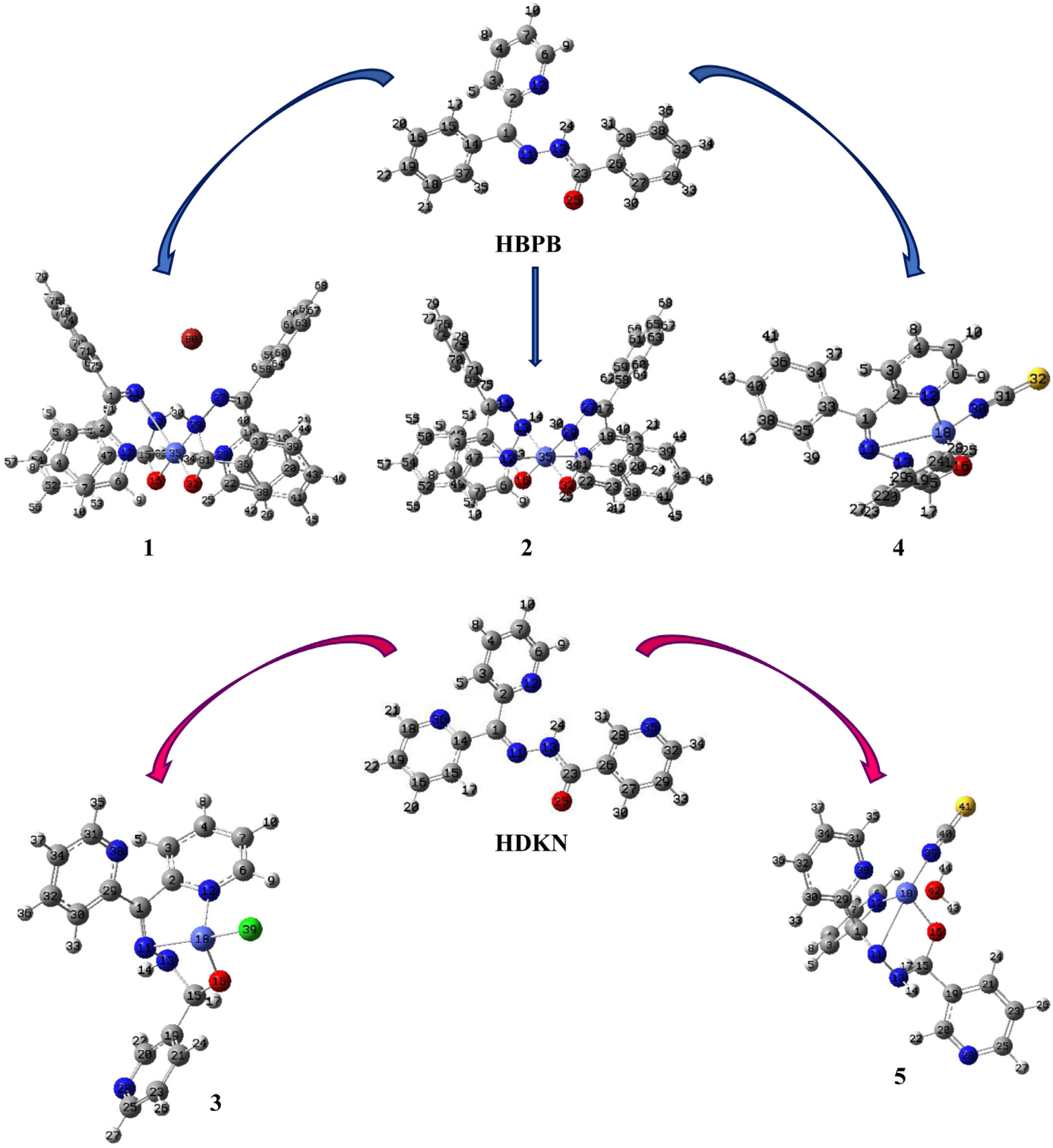

Fig. 7. The optimized structures of the ligands and five cobalt complexes at HF/6-311G(d,p)/LANL2DZ level.

4. Conclusions

The article reports the synthesis and characterization of five cobalt complexes derived from two different aroylhydrazones. In all the complexes the hydrazones were found to be coordinated to the metal center in a similar approach of a tridentate NNO donor type. One of the complexes got crystallized in a distorted octahedral geometry. The complex $[Co(BPB)_2]Br$ is found to be ionic in nature and is diamagnetic. This was evident from molar conductivity studies and magnetic susceptibility measurements. Besides, the NBO calculations revealed that the resonance interactions are mainly responsible for lowering the energy for all complexes. The reactivity analyses made with the help of well-known electronic structure principles like maximum hardness, minimum electrophilicity, and minimum polarizability principles showed that the most stable cobalt complex among studied complexes is com-

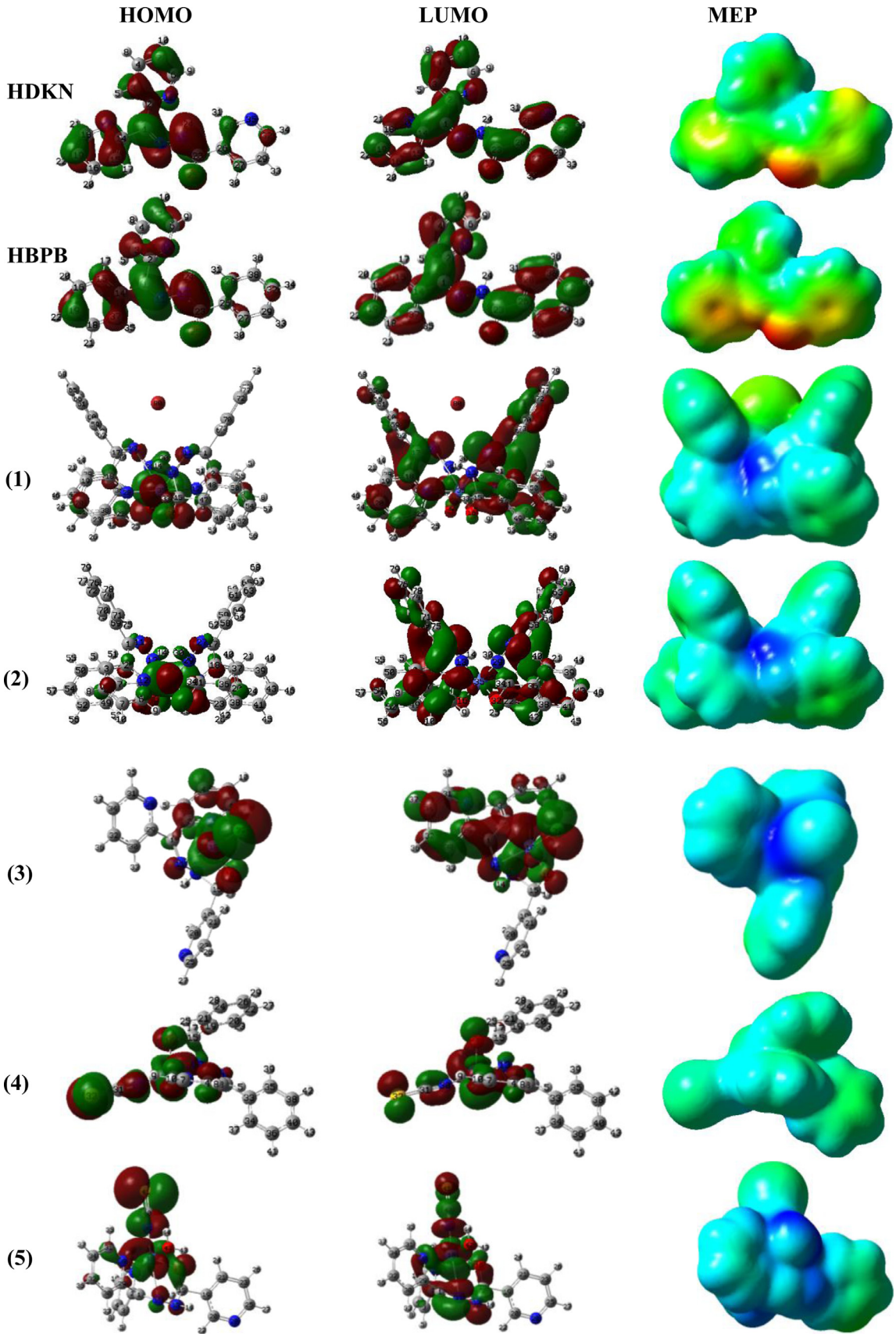

Fig. 8. HOMO & LUMO (isoval:0.02) and MEP (isoval:0.0004) for ligands and cobalt complexes at HF/6-311G(d,p)/LANL2DZ in the gas phase.

Table 6
The quantum chemical reactivity identifiers, total electronic and free energies of the cobalt complexes at HF/6-311G(d,p)/LANL2DZ in the gas phase.

	HBPB	HDKN	1	2	3	4	5
HOMO (-I)	−0.30721	−0.31583	−0.41543	−0.41471	−0.43513	−0.44328	−0.42271
LUMO (-A)	0.07202	0.06879	−0.04983	−0.04875	−0.14871	−0.12031	−0.08207
ΔE (L-H)	10.31938	10.46605	9.94849	9.95828	7.79389	8.78847	9.26929
χ	−3.19992	−3.36115	−6.33019	−6.30570	−7.94355	−7.66804	−6.86789
η	5.15969	5.23302	4.97424	4.97914	3.89694	4.39423	4.63465
ω	0.99226	1.07943	4.02788	3.99284	8.09609	6.69045	5.08861
ΔNmax	0.62018	0.64230	1.27259	1.26642	2.03841	1.74502	1.48186
μ (debye)	6.75063	3.32804	1.75143	0.76902	10.57498	7.27095	10.91801
α (au)	217.47133	207.53467	441.90800	430.03733	237.76633	268.76067	257.69933

*The abbreviations are followed as I, ionization energy; A, electron affinity, ΔE, energy gap; χ, electronic chemical potential; η, global hardness; ω, electrophilicity index; ΔNmax, charge transfer capability; μ, dipole moment; α, polarizability.

plex **2**. Also, HOMO, LUMO, and MEP plots imply that the substituent group (-NCS) and atoms (Br and Cl) chelated to Co atom shifted the chemical reactive site for the complexes.

Author statement

Neema Ani Mangalam: Investigation, Writing
M. R. Prathapachandra Kurup: Conceptualization, Methodology, Supervision, Review, Editing
Eringathodi: XRD analysis
Savaş Kaya: Software, Formal analysis, visualization, Writing
Goncagül Serdaroğlu: Software, Formal analysis, visualization, Writing

Declaration of Competing Interest

There are no conflits of interest.

Acknowledgments

The authors are thankful to the Sophisticated Analytical Instrument Facility, CUSAT, Kochi, India for CHN analysis and NIIST, Trivandrum for providing the NMR spectra of ligands. All calculations have been carried out at TUBITAK ULAKBIM, High Performance and Grid Computing Center (TR-Grid e-Infrastructure).

Supplementary materials

Supplementary material associated with this article can be found, in the online version, at doi:10.1016/j.molstruc.2021.129978.

References

[1] P.H.O. Santiago, M.B. Santiago, C.H.G. Martins, C.C. Gatto, Copper(II) and zinc(II) complexes with Hydrazone: synthesis, crystal structure, Hirshfeld surface and antibacterial activity, Inorg. Chim. Acta 508 (2020) 119632-11963, doi:10.1016/j.ica.2020.119632.
[2] C.C. Carmona-Vargas, I.Y. Váquiro, L.M. Jaramillo-Gómez, J.-M. Lehn, M.N. Chaur, Grid-type complexes of M^{2+} (M = Co, Ni, and Zn) with highly soluble bis(hydrazone)thiopyrimidine-based ligands: spectroscopy and electrochemical properties, Inorg. Chim. Acta 468 (2017) 131–139, doi:10.1016/j.ica.2017.05.002.
[3] N.A. Mangalam, S. Sivakumar, S.R. Sheeja, M.R.P. Kurup, E.R.T. Tiekink, Chemistry of molecular and supramolecular structures of vanadium(IV) and dioxygen-bridged V(V) complexes incorporating tridentate hydrazone ligands, Inorg. Chim. Acta 362 (2009) 4191–4197, doi:10.1016/j.ica.2009.06.029.
[4] C. Wang, N. Xing, W. Feng, S. Guo, Z. You, New mononuclear dioxidomolybdenum(VI) complexes with hydrazone ligands: synthesis, crystal structures and catalytic performance, Inorg. Chim. Acta 486 (2019) 625–633, doi:10.1016/j.ica.2018.11.020.
[5] B. Shaabani, A.A. Khandar, N. Ramazani, M. Flek, H. Mobaiyen, L. Cunha-Silva, Chromium(III), manganese(II) and iron(III) complexes based on hydrazone Schiff-base and azide ligands: synthesis, crystal structure and antimicrobial activity, J. Coord. Chem. 70 (2016) 696–708, doi:10.1080/00958972.2016.1274028.
[6] A.A.R. Despaignea, F.B. Da Costa, O.E. Piro, E.E. Castellano, S.R.W. Louro, H. Beraldo, Complexation of 2-acetylpyridine- and 2-benzoylpyridine-derived hydrazones to copper(II) as an effective strategy for antimicrobial activity improvement, Polyhedron 38 (2012) 285–290, doi:10.1016/j.poly.2012.03.017.
[7] A.A. El-Sherif, A. Fetoh, Y.Kh Abdulhamed, G.M.A. El-Reash, Synthesis, structural characterization, DFT studies and biological activity of Cu(II) and Ni(II) complexes of novel hydrazone, Inorg. Chim. Acta 480 (2018) 1–15, doi:10.1016/j.ica.2018.04.038.
[8] A.A. Khandar, Z.M. Azar, M. Eskandani, C.B. Hubschle, S. van Smaalen, B. Shaabani, Y. Omidi, Cadmium(II) complexes of a hydrazone ligand: synthesis, characterization, DNA binding, cyto- and genotoxicity studies, Polyhedron 171 (2019) 237–248, doi:10.1016/j.poly.2019.06.026.
[9] S. Mondal, C. Das, B. Ghosh, B. Pakhira, A.J. Blake, M.G.B. Drew, S.K. Chattopadhyay, Synthesis, spectroscopic studies, X-ray crystal structures, electrochemical properties and DFT calculations of three Ni(II) complexes of aroylhydrazone ligands bearing anthracene moiety, Polyhedron 80 (2014) 272–281, doi:10.1016/j.poly.2014.05.028.
[10] H.H. Monfared, S. Kheirabadi, N.A. Lalami, P. Mayer, Dioxo- and oxovanadium(V) complexes of biomimetic hydrazone ONO and NNS donor ligands: synthesis, crystal structure and catalytic reactivity, Polyhedron 30 (2011) 1375–1384, doi:10.1016/j.poly.2011.02.005.
[11] P. Singh, A.K. Singh, V.P. Singh, Synthesis, structural and corrosion inhibition properties of some transition metal(II) complexes with o-hydroxyacetophenone-2-thiophenoyl hydrazone, Polyhedron 65 (2013) 73–81, doi:10.1016/j.poly.2013.08.008.
[12] O.A. El-Gammal, Mononuclear and binuclear complexes derived from hydrazone Schiffbase NON donor ligand: synthesis, structure, theoretical and biologicalstudies, Inorg. Chim. Acta 435 (2015) 73–81, doi:10.1016/j.ica.2015.06.009.
[13] G.M. Sheldrick, ActaCryst C71 (2015) 3–8, doi:10.1107/S2053229614024218.
[14] K. Brandenburg, Diamond Version 3.1f, Crystal Impact GbR, Bonn, Germany, 2008.
[15] M.J. Frisch, G.W. Trucks, H.B. Schlegel, G.E. Scuseria, M.A. Robb, J.R. Cheeseman, G. Scalmani, V. Barone, B. Mennucci, G.A. Petersson, H. Nakatsuji, M. Caricato, X. Li, H.P. Hratchian, A.F. Izmaylov, J. Bloino, G. Zheng, J.L. Sonnenberg, M. Hada, M. Ehara, K. Toyota, R. Fukuda, J. Hasegawa, M. Ishida, T. Nakajima, Y. Honda, O. Kitao, H. Nakai, T. Vreven, J.A. Montgomery Jr., J.E. Peralta, F. Ogliaro, M. Bearpark, J.J. Heyd, E. Brothers, K.N. Kudin, V.N. Staroverov, T. Keith, R. Kobayashi, J. Normand, K. Raghavachari, A. Rendell, J.C. Burant, S.S. Iyengar, J. Tomasi, M. Cossi, N. Rega, J.M. Millam, M. Klene, J.E. Knox, J.B. Cross, V. Bakken, C. Adamo, J. Jaramillo, R. Gomperts, R.E. Stratmann, O. Yazyev, A.J. Austin, R. Cammi, C. Pomelli, J.W. Ochterski, R.L. Martin, K. Morokuma, V.G. Zakrzewski, G.A. Voth, P. Salvador, J.J. Dannenberg, S. Dapprich, A.D. Daniels, O. Farkas, J.B. Foresman, J.V. Ortiz, J. Cioslowski, D.J. FoxGaussian, Inc., Wallingford CT, Gaussian 09 D.01, Gaussian, Inc, Wallingford CT, 2013.
[16] C.C.J. Roothaan, New developments in molecular orbital theory, Rev. Mod. Phys. 23 (1951) 69, doi:10.1103/RevModPhys.23.69.
[17] F. Weinhold, C.R. Landis, E.D. Glendening, What is NBO analysis and how is it useful? Int. Rev. in Phys. Chem. 35 (2016) 399–440, doi:10.1080/0144235X.2016.1192262.
[18] A.E. Reed, L.A. Curtiss, F. Weinhold, Intermolecular interactions from a natural bond orbital, donor-acceptor viewpoint, Chem. Rev. 88 (1988) 899, doi:10.1021/cr00088a005.
[19] T. Koopmans, Über die Zuordnung von Wellenfunktionen und Eigenwerten zu den Einzelnen Elektronen Eines Atoms, T. Physica. 1 (1934) 104–113, doi:10.1016/S0031-8914(34)90011-2.
[20] R.G. Parr, L.V. Szentpaly, S. Liu, Electrophilicity index, J. Am. Chem. Soc. 121 (1999) 1922–1924, doi:10.1021/ja983494x.
[21] R.G. Parr, R.G. Pearson, Absolute hardness: companion parameter to absolute electronegativity, J. Am. Chem. Soc. 105 (1983) 7512–7516, doi:10.1021/ja00364a005.
[22] N. Islam, S. Kaya, Conceptual Density Functional Theory and Its Application in the Chemical Domain, Eds., CRC Press, 2018.
[23] T. Tsuneda, J.W. Song, S. Suzuki, K. Hirao, On Koopmans' theorem in density functional theory, J. Chem. Phys. 133 (17) (2010) 174101, doi:10.1063/1.3491272.

[24] R.G. Parr, L.V. Szentpaly, S. Liu, Electrophilicity index, J. Am. Chem. Soc. 121 (9) (1999) 1922–1924, doi:10.1021/ja983494x.
[25] P.K. Chattaraj, S. Duley, L.R. Domingo, Understanding local electrophilicity/nucleophilicity activation through a single reactivity difference index, Org. Biomol. Chem. 10 (14) (2012) 2855–2861, doi:10.1039/C2OB06943A.
[26] Gaus View 6.0.16, Gaussian, Inc, Wallingford CT, 2016.
[27] N. Mathew, M.R.P. Kurup, Synthesis and characterization of Mo(VI) complexes derived from ONO donor acylhydrazones, Spectrochim. Acta A 78 (2011) 1424–1428, doi:10.1016/j.saa.2011.01.021.
[28] N. Bouslimani, N. Clement, G. Rogez, P. Turek, S. Choua, S. Dagorne, R. Welter, Stability, molecular structures and magnetic properties of dinuclear iron complexes supported by benzoic hydrazide derivative ligands, Inorg. Chim. Acta 363 (2010) 213–220, doi:10.1016/j.ica.2009.08.027.
[29] N.A. Mangalam, S.R. Sheeja, M.R.P. Kurup, Mn(II) complexes of some acylhydrazones with NNO donor sites: syntheses, a spectroscopic view on their coordination possibilities and crystal structures, Polyhedron 29 (2010) 3318–3323, doi:10.1016/j.poly.2010.09.007.
[30] A. Ray, S. Banerjee, S. Sen, R.J. Butcher, G.M. Rosair, M.T. Garland, S. Mitra, Two Zn(II) and one Mn(II) complexes using two different hydrazone ligands: spectroscopic studies and structural aspects, Struct. Chem. 19 (2008) 209–217.
[31] P. Bindu, M.R.P. Kurup, Spectrochemical studies of iron(III) and cobalt(II) complexes of salicylaldehyde N(4)- phenyl thiosemicarbazones with heterocyclic bases, Indian J. Chem. 38A (1999) 388–391 http://nopr.niscair.res.in/handle/123456789/15662.
[32] N.A. Mangalam, S. Sivakumar, M.R.P. Kurup, E. Suresh, Design and characterization of Cu(II) complexes from 2-benzoylpyridine benzhydrazone: crystallographic evidence for coordination versatility, Spectrochim. Acta A 75 (2010) 686–692, doi:10.1016/j.saa.2009.11.040.
[33] M. Abedi, O.Z. Yeşilel, G. Mahmoudi, A. Bauzá, Y. Yerli, W. Kaminsky, P. Garczarek, J.K. Zaręba, Andrea Ienco, M.S. Gargari, Tetranuclear manganese(II) complexes of hydrazone and carbohydrazone ligands: synthesis, crystal structures, magnetic properties, Hirshfeld surface analysis and DFT calculations, Inorg. Chim. Acta 443 (2016) 101–109, doi:10.1016/j.ica.2015.12.012.
[34] K.U. Ambili, M. Sithambaresan, M.R.P. Kurup, Interplay of bifurcated hydrogen bonds in making of inclusion/pseudo-inclusion complexes of Ni(II), Cu(II) and Zn(II) of a salophen type ligand: crystal structures and spectral aspects, J. Mol. Struct. 1134 (2017) 687–696, doi:10.1016/j.molstruc.2016.12.103.
[35] W.J. Geary, The use of conductivity measurements in organic solvents for the characterisation of coordination compounds, Coord. Chem. Rev. 7 (1971) 109, doi:10.1016/S0010-8545(00)80009-0.
[36] A. Bayri, A.R. Bahadır, F.M. Avcu, O.¨. Aytekin, Surprising magnetic behavior of cobalt(II) ion in recently prepared macrocycle complexes. Distortion versus intermolecular antiferromagnetic exchange interactions, Transit Met. Chem. 30 (2009) 987–991, doi:10.1007/s11243-005-6313-3.
[37] A.A.A. Abu-Hussen, W. Linert, Redox, thermodynamic and spectroscopic of some transition metal complexes containing heterocyclic Schiff base ligands, Spectrochim. Acta Part A 74 (2009) 214–223, doi:10.1016/j.saa.2009.06.023.
[38] K. Roztocki, D. Matoga, W. Nitek, Cobalt(II) compounds with acetone isonicotinoyl hydrazone tautomers: syntheses and crystal structures of complexes with free donor atoms, Inorg. Chim. Acta 448 (2016) 86–92, doi:10.1016/j.ica.2016.03.045.
[39] M.C. Vineetha, M. Sithambaresan, Y.S. Nair, M.R.P. Kurup, Structural investigation of discrete solvent protonated vanadium and other transition metal complexes of N'-[(E)-(3-ethoxy-2-hydroxyphenyl) methylidene]benzohydrazide, synthetic, spectroscopic and cytotoxicity studies, Inorg. Chim. Acta 491 (2019) 93–104, doi:10.1016/j.ica.2019.03.040.
[40] T.M. Asha, M.R.P. Kurup, Synthesis, spectral characterization and crystal structures of dioxidomolybdenum(VI) complexes derived from nicotinoylhydrazones, J. Chem. Crystallogr. 49 (2019) 219–231, doi:10.1007/s10870-018-0756-9.
[41] J.E. Philip, M. Shahid, M.R.P. Kurup, M.P. Velayudhan, Metal based biologically active compounds: design, synthesis, DNA binding and antidiabetic activity of 6-methyl-3-formyl chromone derived hydrazones and their metal(II) complexes, J. Photochem. Photobiol. B 175 (2017) 178–191, doi:10.1016/j.jphotobiol.2017.09.003.
[42] L.Y. He, X.-Y. Qiu, J.-Y. Cheng, S.-J. Liu, S.-M. Wu, Synthesis, characterization and crystal structures of vanadium(V) complexes derived from halido-substituted tridentate hydrazone compounds with antimicrobial activity, Polyhedron 156 (2018) 105–110, doi:10.1016/j.poly.2018.09.017.
[43] R. Venugopal, S.S. Sreejith, M.R. Kurup, Crystallographic, spectroscopic and theoretical investigations on Ni(II) complexes of a tridentate NNS donor thiosemicarbazone, Polyhedron 158 (2019) 398–407, doi:10.1016/j.poly.2018.11.023.
[44] B.S. Garg, M.R.P. Kurup, S.K. Jain, Y.K. Bhoon, Characterization of nickel(II) complexes of substituted 2-acetylpyridine thiosemicarbazones, Transit. Met. Chem. 16 (1991) 111–113, doi:10.1007/BF01127883.
[45] N. Aiswarya, M. Sithambaresan, S.S. Sreejith, S. Weng Ng, M.R.P. Kurup, Polymeric polymorphs and a monomer of pseudohalide incorporated Cu(II) complexes of 2,4-dichlorido-6-((2-(dimethylamino)ethylimino)methyl)phenol]: crystal structures and spectroscopic behaviour, Inorg. Chim. Acta 443 (2016) 251–266, doi:10.1016/j.ica.2016.01.008.
[46] M. Sutradhar, T.R. Barman, J. Klanke, M.G.B. Dreb, E. Rentschler, A novel Cu(II) dimer containing oxime-hydrazone Schiff base ligands with an unusual mode of coordination: study of magnetic,autoreduction and solution properties, Polyhedron 53 (2013) 48–55, doi:10.1016/j.poly.2012.12.039.
[47] C. Gökçe, N. Dilek, R. Gup, Seven coordinated cobalt(II) complexes with 2,6-diacetylpyridine bis(4-acylhydrazone) ligands: synthesis, characterization, DNA-binding and nuclease activity, Inorg. Chim. Acta 432 (2015) 213–220, doi:10.1016/j.ica.2015.03.040.
[48] A.B.P. Lever, Inorganic Electronic Spectroscopy, 2nd ed., Elsevier, Amsterdam, 1984.
[49] A. Datta, P.-H. Liu, J.-H. Huang, E. Garribba, M. Turnbull, B. Machura, C.-L. Hsu, W.-T. Chang, A. Pevec, End-to-end thiocyanato-bridged zig-zag polymers of Cu^{II}, Co^{II} and Ni^{II} with a hydrazone ligand: EPR, magnetic susceptibility and biological study, Polyhedron 44 (2012) 77–87, doi:10.1016/j.poly.2012.06.027.
[50] V. Suni, M.R.P. Kurup, M. Nethaji, Studies on Co(II) and Co(III) complexes of di-2-pyridyl ketone N(4)-cyclohexyl and N(4)-phenyl thiosemicarbazones, Polyhedron 26 (2007) 5203–5209, doi:10.1016/j.poly.2007.07.051.
[51] S. Kaya, C. Kaya, A simple method for the calculation of lattice energies of inorganic ionic crystals based on the chemical hardness, Inorg. Chem. 54 (2015) 8207–8213, doi:10.1021/acs.inorgchem.5b00383.
[52] S. Kaya, C. Kaya, N. Islam, Maximum hardness and minimum polarizability principles through lattice energies of ionic compounds, Physica B 485 (2016) 60–66, doi:10.1016/j.physb.2016.01.010.
[53] S. Pan, M. Solà, P.K. Chattaraj, On the validity of the maximum hardness principle and the minimum electrophilicity principle during chemical reactions, J. Phys. Chem. A 117 (8) (2013) 1843–1852, doi:10.1021/jp312750n.
[54] S. Kaya, C. Kaya, A new method for calculation of molecular hardness: a theoretical study, Comput. Theor. Chem. 1060 (2015) 66–70, doi:10.1016/j.comptc.2015.03.004.

Adhesion in Biocomposites: A Critical Review

Authors: Mary, Siji K.; Thomas, Merin Sara; Koshy, Rekha Rose; Pillai, Prasanth K.S.; Pothan, Laly A.; Thomas, Sabu
Source: Reviews of Adhesion and Adhesives, Volume 8, Number 4, December 2020, pp. 527-553(27)
Publisher: Scrivener Publishing
DOI: https://doi.org/10.7569/RAA.2020.097312

Abstract | References | Citations | Supplementary Data

Environmental concerns and increasing awareness about sustainability issues are driving the push to develop bio-based composites from renewable and sustainable resources. A clear understanding of fiber-matrix interaction at the interfaces is vital for the design and production of these composite materials because stress transfer between load-bearing fibers occurs at these interfaces, and this can determine their mechanical and thermal behaviors. A detailed study of different attributes such as processing technology parameters, types of biopolymers, and chemical and physical treatments is essential to effect interface modification and facilitate a better understanding of these composites from an application perspective. In this article, we attempt to critically review adhesion in biocomposites with special emphasis on the effects of various surface modifications and the processing technology adopted. The review also addresses various characterization techniques adopted for evaluating adhesion in biocomposites.

Keywords: ADHESION; BIOCOMPOSITES; BIOPOLYMER; CHEMICAL MODIFICATION; DIFFUSION; INTERFACE
Document Type: Research Article
Publication date: December 1, 2020

Functionalized Polymers (https://www.taylorfrancis.com/books/mono/10.1201/9780367821913/functionalized-polymers?refId=5cad300b-555b-44e4-9d83-3d31a025969f&context=ubx)

Show Path

Chapter

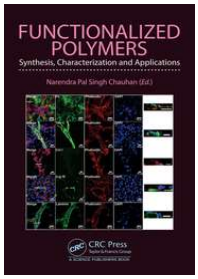

Functionalization of Cellulose—Chemical Approach

By Merin Sara Thomas, Prasanth K.S. Pillai, Sabu Thomas, Laly A. Pothen

Book Functionalized Polymers (https://www.taylorfrancis.com/books/mono/10.1201/9780367821913/functionalized-polymers?refId=5cad300b-555b-44e4-9d83-3d31a025969f&context=ubx)

Edition	1st Edition
First Published	2021
Imprint	CRC Press
Pages	14
eBook ISBN	9780367821913

ABSTRACT

< Previous Chapter (chapters/edit/10.1201/9780367821913-6/functional-proteins-keya-ganguly-ki-taek-lim?context=ubx)
Next Chapter > (chapters/edit/10.1201/9780367821913-8/functionalized-polymers-processed-3d-printing-narendra-pal-singh-chauhan-mahrou-sadri-behnaz-sadat-eftekhari-behnaz-sadat-eftekhari-farzin-sahebjam-mazaher-gholipourmalekabadi-mazaher-gholipourmalekabadi?context=ubx)

(/)

Policies

Journals

Corporate

Help & Contact

Connect with us

(https://www.linkedin.com/company/taylor-&-francis-group/)

(https://twitter.com/tandfnewsroom?lang=en)

(https://www.facebook.com/TaylorandFrancisGroup/)

(https://www.youtube.com/user/TaylorandFra

IJARSCT
ISSN (Online) 2581-9429
ISSN (Print) 2581-XXXX
International Journal of Advanced Research in Science, Communication and Technology (IJARSCT)
Volume 11, Issue 2, November 2020
Impact Factor: 4.819

Effect of Counterions on Cation…π Interactions

Dr. Sharon Achamma Abraham
Department of Chemistry
Mar Thoma College, Tiruvalla, Kerala, India

Abstract: *Counterions like F^-,Cl^-.Br^-,I^- are introduced into benzene…Li^+, benzene….Na^+ and benzene…K^+ complexes. Addition of these counterions lowers the binding energy of these cation…π systems. The alkali metal cations includingLi^+,Na^+ and K^+ and counterions including F^-,Cl^-,Br^-,I^- are considered in the present study usingB3LYP/6-31+G(d,p)basis set. Results show that cation….π interactions are more stable than counter ionic interactions. When counterions like halide ions, sulphate ions and phosphate ions are introduced into a cation….π complex, there observed a decrease in binding energy, which yields valuable information in understanding crystal packing.*

I. Introduction

Benzene can be considered as a planar hexagonal system with delocalized π electron centres above and below the plane . Addition or Interaction of a cation reduces the charge density on the benzene. The cation binds to the π-face of the aromatic. In the initial findings, K^+ interacts with water gives an interaction energy of 18kcal/mol, where as K^+ with benzene it is 19 kcal/mol [1]. Hence the aromatic complexes are more stronger. Both NMe_4^+ and K^+ have similar interaction energies. Electrostatic interaction is the driving force for these interactions.[2]

It is seen that a counterion is the ion ,that accompanies an ionic species inorder to maintain electric neutrality.[3,4,5]. In Sodium chloride(NaCl), the sodium cation is the counterion for the chlorine atom and vice versa. In tight ion pairs, the anion will effect the ability of the cation to participate in cation….π binding. In tetramethylammonium binding with picrate, the binding energy is for picrate is found to be -8.35kcal/mol, in tetramethylammonium chloride, the binding energy for chloride is -4.64kcal/mol. Results shows that cation-π interactions are more stable than counterionic interactions. (Alkali metals> Alkaline earth metals.) When counterions like halogens, sulphates and phosphates are introduced into a cation-π complex, there is a decrease in binding energy.

II. Theory of Cation–ii Interactions

Electrostatic model and Quadrople moment are the important factors controlling cation…π Interactions . According to electrostatic model, the positive surface is balanced by negative π-Electrons above and below the plane. A comparison of simple alkali metals binding to Benzene, the trend is Li^+ > Na^+> K^+ gives -37.24kcal/mol, -24.06kcal/mol and -15.23kcal/mol. The more negative the maximum electron charge cloud over the center of the aromatic, cation-π interaction is stronger.

Electrostatic components and dispersive forces are one of the major factor, that controls cation- π interaction. Probably the most important of these for simple systems is the interaction of the ion with the induced dipole in the system. Donor-acceptor and charge- transfer terms along with dispersion forces may also be important.

Binding Energy is one of the factor that controls Cation π interaction. It is found that when the binding energy of cation….π system is more negative, it is more stable.The electrostatic forces and dispersion forces are also interesting. The role of an induced dipole in cation binding showed that cyclohexane is better than benzene in this regards it is just that the induced dipole is not enough to make a strong cation binding site.

Concerning the aromatic component, the electrostatic potential surfaces of the aromatic rings of delocalization electron clouds shows trends in cation-π interactions. Variations among the ions are also consistent, in that the cation-π interaction decreases as the ionic radius increases, as expected for an electrostatic model.

Benzene, has no dipole moment, but it does have a substantial, permanent quadrupole moment. A quadrupole can be thought of as two dipoles aligned in such a way so that there is no net dipole. Topologically, quadrupoles are equivalent to dorbitals and the quadrupole in benzene in particular is topologically equivalent to a dz^2 orbital. Thus, there is a

IJARSCT
ISSN (Online) 2581-9429
ISSN (Print) 2581-XXXX
International Journal of Advanced Research in Science, Communication and Technology (IJARSCT)
Volume 11, Issue 2, November 2020
Impact Factor: 4.819

permanent, non-spherical charge distribution in benzene, with regions of relative negative and positive charges. Plots of the electrostatic potential surface provide a useful way to visualize the quad-rupole. Just as an ion can be attracted to the appropriate end of a dipole, so can an ion experience a favourable interaction with appropriate regions of a quadrupole. This is an electrostatic interactions ,it requires no adjustment of the electronic distribution around the ion or the molecule. Importantly, there is no a prior reason to expect that such interactions will be inherently weaker when the molecule contributes a quadrupole rather than a dipole.

The usefulness of the quadrupole moment is that it provides an easy way to visualize the charge distribution of aromatics and leads naturally to the expectation of significant electrostatic interactions. It also correctly predicts the preferred geometries of cation-π complexes and other "polar-π" inter- actions.

III. Structure and Bonding

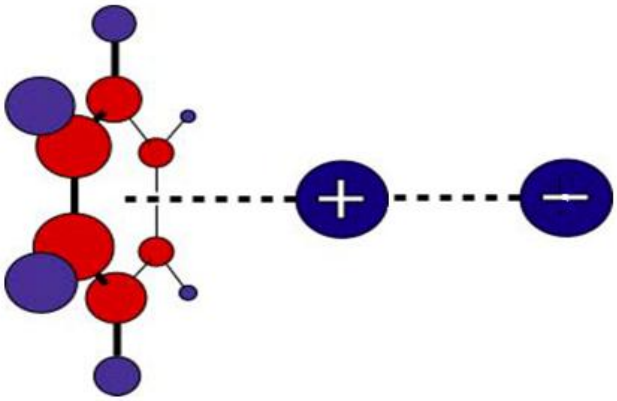

IV. Cation…ii Interactions-Counterionic Effect

SO_4^{2-} ion is a counterionic group, it is interacted with the benzene…Li^+ system. It is seen that the cation-π system is interacting with the counterionic system. The sulphur oxygen bond aligned parallel to the carbon hydrogen bond. When benzene…Li^+ system interacts with the counterionic group like SO_4^{2-}system, through non-covalent interaction, there forms interaction energy. This counterionic interactions forms a planar system, where as in Li^+ ion, cation Pi interaction exists.

Six resonances can possible for an sulfate ion. The SO_4^{2-} exists in the resonance forms, where the sulphur-oxygen bond has more energy than the oxygen- oxygen bond. The S-O bond length is 2Angstrom more. Many Interactions are possible in these type of systems. The S-O bond length is 2Angstrom more than O-O bond or S-S bond.

A) Sulfateion (SO_4^{2-})

Sulfate ion (SO_4^{2-}) is the conjugate base of HSO_4^-, which in turn is the conjugate base of H_2SO_4, sulphuric acid. GilbertLewisin1916, in terms of electron octets around each atom, proposed that there is no double bonds but only aformalchargeof2+onthesulphuratom. The apparent contradiction to the shortness of the S-O bond length insulfateion than S-O single bonds can be cleared if one realizes that there are covalent double bonds in the Lew is structure that representbondsthatarestronglypolarizedbymorethan90%towardstheoxygenatom.Ontheotherhand,inthestructurewithanio nicbond,thechargeislocalizedasalonepairontheoxygen.

B) Phosphate ion (PO_4^{3-})

The phosphate ion is a polyatomic ion with the empirical formula PO_4^{3-} and a molar mass of 94.97 g/mol. It consists of one central phosphorus atom surrounded by four oxygen atoms in a tetrahedral arrangement. The phosphate ion carries a negative three formal charge and is of the hydrogen phosphate ion, HPO_4^{2-} , which is the conjugate base of

IJARSCT
ISSN (Online) 2581-9429
ISSN (Print) 2581-XXXX
International Journal of Advanced Research in Science, Communication and Technology (IJARSCT)
Volume 11, Issue 2, November 2020
Impact Factor: 4.819

$H_2PO_4^-$, the dihydrogen phosphateion, which in turn is the conjugate base of H^3PO^4, phosphoric acid. A phosphate salt forms when a positively charged ion attaches to the negatively charged oxygen atoms of the ion, forming an ionic compound.

C) Chlorate (ClO_3^-)

The chlorate ion cannot be satisfactorily represented by just one Lewis structure since all the Cl-O bonds are of the same length (1.49 Å) in potassium chlorate and the chlorine atom is hypervalent. Instead, it is often thought of as a hybrid of multiple resonance structures.

V. COUNTERION EFFECT IN CATION-II SYSTEMS

Counterions like F^-, Cl^-, Br^-, I^-_ are introduced into benzene...Li^+, benzene....Na^+ and benzene...K^+ complexes. Addition of these ions lowers the binding energy. Binding energy shows an increase in the values, from F^- to I^-. Cation-π interaction with counterionic groups are strongly favoured when an anion like I^- is interacting. The binding energy is found to be -25.63kcal/mol. The observed values are found to be -13.98,-15.21,-16.67 and -25.63 kcal/mol.[6,7,8]. Calculations were performed on the interaction between cation…π systems and various anionic groups, which are called counterionic groups, where M+=Li+,Na+,K+ and X=F-,Cl-,Br-.I^-.Calculations were performed using B3LYP version of DFT. 6-31+G(d,p) basis set was employed. Calculations for the lowest energy structures were obtained.

It is observed that the cation…π interaction in benzene…..Li^+, benzene….Na^+, Benzene..K^+ systems are more stronger than counterionic interactions. Electrostatic interaction is the major driving force for benzene…Li^+, Na^+, K^+ complexes where charge transfer decreases in the order K^+>Na^+>Li^+

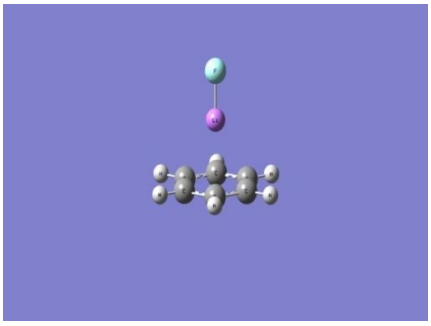

Benzene……Li+…..

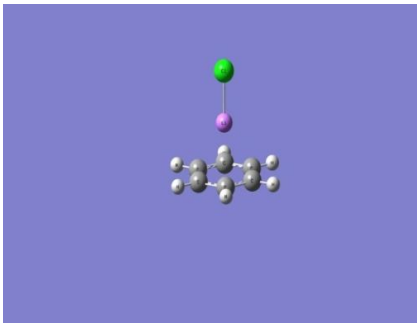

F-Benzene…..Li+……Cl-

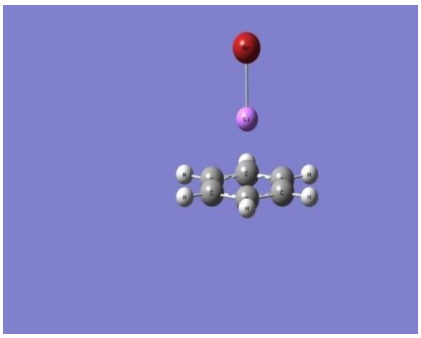

Benzene……Li+……

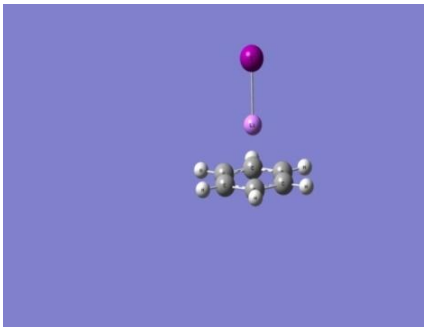

Br-Benzene…….Li+……I-

Benzene..Li^+halide counterionic systems

IJARSCT
ISSN (Online) 2581-9429
ISSN (Print) 2581-XXXX
International Journal of Advanced Research in Science, Communication and Technology (IJARSCT)
Volume 11, Issue 2, November 2020
Impact Factor: 4.819

Counterionic Systems	ΔE(kcal/mol)	ΔE_{bsse}(kcal/mol)
Benz…..Li^+F^-	-13.98kcal/mol	-11.57kcal/mol
Benz….Li^+Cl^-	-15.21kcal/mol	-13.38kcal/mol
Benz….Li^+Br^-	-16.67kcal/mol	-13.46kcal/mol
Benz…..Li^+I^-	-25.63kcal/mol	-16.42kcal/mol

Binding Energy of Benzene..M^+halide counterionic systems

Counterionic System	**ΔE(kcal/mol)**	**ΔE_{bsse}(kcal/mol)**
Benz….Na^+F^-	-9.76kcal/mol	-9.03kcal/mol
Benz….Na^+Cl^-	-10.64kcal/mol	-9.96kcal/mol
Benz….Na^+Br^-	-13.26kcal/mol	-9.88kcal/mol
Benz…..Na^+I^-	-14.06kcal/mol	-5.84kcal/mol
Benz…..K^+F^-	-6.64kcal/mol	-6.15kcal/mol
Benz….K^+Cl^-	-7.13kcal/mol	-6.41kcal/mol
Benz…..K^+Br^-	-9.27kcal/mol	-6.12kcal/mol
Benz…..K^+I^-	-15.62kcal/mol	-5.41kcal/mol

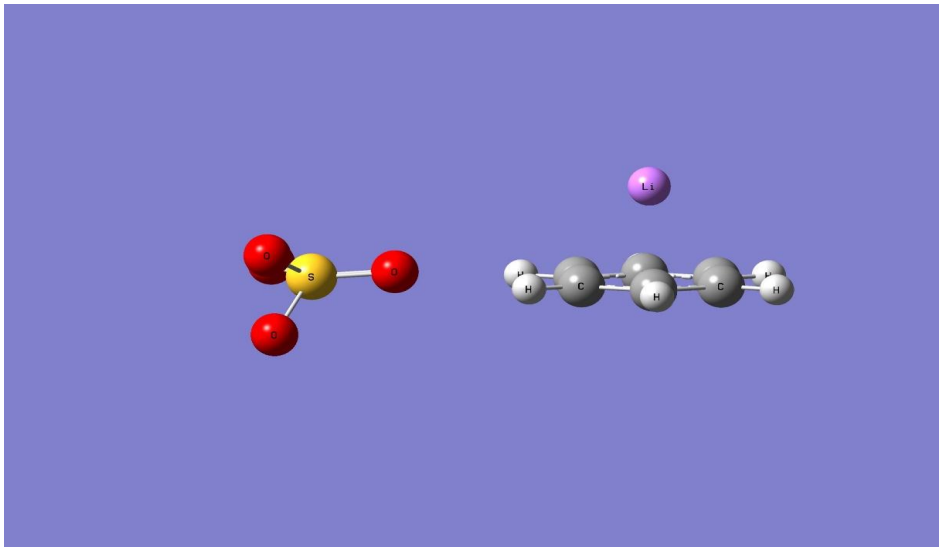

In benzene.....Li^+ sulfate, there is some interaction energy.(82kcal/mol).There is no such interaction in Na^+ and K^+. In benzene.....Li^+ chlorate, there is no binding of chlorate with Li. It is not in Na^+ and K^+. In benzene....Li^+ phosphate, phosphate binds with Li+ and not in Na^+ and K^+.

In Benzene.....Li phosphate , the Li^+ ion binds with central phosphorus atom significantly a Li-P bond, with the Li attached to two oxygen atoms. P=O bond perpendicular to the plane, above the counterionic system. It is similar to a diamond shaped cut. The oxygen-Lithium bond lengths are 2.5 angstroms and 2.4 angstrom. Binding energy is decreased Li^+ above the plane binds to the aromatic ring .It shows a binding energy of 82kcal/mol where as reverse in the case of Na+ and K^+. The counterionic bond is not seen in the benzene....Na+ phosphate. It is not at all binding in K^+.

IJARSCT
ISSN (Online) 2581-9429
ISSN (Print) 2581-XXXX
International Journal of Advanced Research in Science, Communication and Technology (IJARSCT)
Volume 11, Issue 2, November 2020
Impact Factor: 4.819

VI. CONCLUSION

Cation….π Interaction with counterionic groups are strongly favoured when an anion like I-Is interacting. Among the halide counterions, Benz…M+I- is more stable.ie, Benz…M+I- binds more and is stable as F<Cl<Br<I. Addition of counter ions like halide ions lowers the binding energy of cation…π system. This study yields valuable information in crystal packing[10,11,12] and also in the transport of ions in biological systems[13]

REFERENCES

[1]. Kebarle, J. Phys. Chem., 1981, 85, (1814)
[2]. Sunner, J.; Nishisawa, K.; Kebarle, P. J.Phys. Chem., 85, 1814-1820(1981)
[3]. Quinonero D.; Garau C.; Rotger C.; Frontera A.; Ballester P.; Costa A.; Deya P. M., Angew. Chem., Int. Ed., 41, 3389–3392(2002)
[4]. de Hoog P.; Gamez P.; Mutikainen H.; Turpeinen U.; Reedijk J. Angew. Chem., Int.Ed, 43, 5815–5817(2004).
[5]. Demeshko S.; Dechert S.; Meyer F., J. Am. Chem. Soc., 126, 4508–4509(2004).
[6]. Laskin, A.; Gaspar, D. J.; Wang, W.-H.;Hunt, S. W.; Cowin, J. P.; Colson, S. D.; Finlayson-Pitts, B. J. Science, 301, 340(2003).
[7]. MacGillivray, L. R.; Atwood, J. L. J. Chem. Soc. Chem. Commun., 44(1997).
[8]. King, B. T.; Noll, B. C.; Michl, J. Collect. Czech. Chem. Commun., 64, 1001 (1999).
[9]. Khademi, S.; O'Connell, J., III; Remis, J.; Robles-Colmenares, Y.;Miercke, L. J. W. Stroud, R. M. Science 305, 1587.(2004).
[10]. Nathanson, G. M.; Davidovits, P.; Worsnop, D. R.; Kolb, C. E. J.Phys. Chem. 100, 13007 (1996). Laskin, A.; Gaspar, D. J.; Wang, W.-H.;Hunt, S. W.; Cowin, J. P.; Colson, S. D.; Finlayson-Pitts, B. J. Science, 301, 340(2003).
[11]. MacGillivray, L. R.; Atwood, J. L. J. Chem. Soc. Chem. Commun.1997, 44. Bodkin, M. J.; Goodfellow, J. M. Protein Sci., 4, 603(1995). Dill,K. A.; Fiebig, K. M.; Chan, H. S. Proc. Natl. Acad. Sci. U.S.A., 90,1942(1993).
[12]. King, B. T.; Noll, B. C.; Michl, J. Collect. Czech. Chem. Commun, 64, 1001(1999).
[13]. Khademi, S.; O'Connell, J., III; Remis, J.; Robles-Colmenares, Y.;Miercke, L. J. W.; Stroud, R. M. Science, 305, 1587(2004).

ISSN (Online) 2456 -1304

International Journal of Science, Engineering and Management (IJSEM)
Vol 6, Issue 10, October 2021

Reorganization Energies of Oligoacenes

Dr.Sharon Achamma Abraham
Assistant Professor, Department of Chemistry, Mar Thoma College, Tiruvalla, Kerala, India
Email: sharon.1384@gmail.com

***Abstract*---The reorganization energies of Oligoacenes from benzene to nonacene were studied using DFT method at B3LYP functional and 6-31+G(d,p) basis set in Gaussian09. Reorganization energy (λ_{hole}) and ($\lambda_{electron}$) from cationic and anionic state are calculated to determine rate of charge transfer and Diffusion coefficient in pair of molecules. The diffusion coefficient is used to determine mobility properties and electronic properties of organic semiconductors. Electron and hole reorganization energies (λ_{hole}) and ($\lambda_{electron}$) decrease with increase in number of benzene rings in oligoacenes and rate of charge transfer increases. Thus oligoacenes act as high mobility and high efficiency organic semiconductors. The calculation of electron and hole Reorganization energies is an important method for determining mobility of organic molecular solids. Oligoacenes with low reorganization energy values can act as high mobility Organic semiconductors for Organic Field effect Transistors. These properties are used to determine mobility properties of Organic Semiconductors. Thus low reorganization energies has applications in designing of materials.**

***Keywords*--- Reorganization energy, Transport property, mobility, Oligoacene**

I. INTRODUCTION

Reorganization energy of oligoacenes is one of its most important Transport property , studied and calculated computationally. It is total sum of inner component reorganization energy and outer component reorganization energy, $\lambda=\lambda_i + \lambda o$. ie, The total reorganization energy of material includes modification of molecular geometry(change in bondlength) as well as surrounding medium due to polarization effect(solvent) with addition and removal of a charge carrier and is expressed as $\lambda=\lambda i + \lambda o$. Here λ_i is inner component reorganization energy and λ_o is outer component reorganization energy.[1,2,3]
htttp://www.iaeme.com/ijaret.asp
Reorganization energies studied on Oligoacenes from benzene to nonacene are calculated in electron volts. These reorganization energies decreases from benzene to nonacene as seen from values given computationally. These calculations are performed using B3LYP functional and 6-31+G(d,p) basis set in Gaussian09. These calculations were based on Marcus theory of equations. Reorganization energy depends upon structure of molecule in neutral state and cationic state.[4]

II. REORGANIZATION ENERGIES FOR OLIGOACENES

Acenes	**λ_{hole}(eV)**	**$\lambda_{electron}$(eV)**
Benzene	0.313	0.249
Naphthalene	0.179	0.235
Anthracene	0.136	0.193
Phenanthrene	0.213	0.304
Tetracene	0.110	0.158
Pyrene	0.149	0.210
Pentacene	0.095	0.129
Hexacene	0.078	0.110
Heptacene	0.068	0.093
Octacene	0.057	0.071
Nonacene	0.049	0.060

These calculations are obtained using B3LYP functional and 6-31+G(d,p) basis set of DFT. In these reorganization energy of oligoacenes, it is observed that bondlengths, structure, plane of the molecule changes for product obtained. The bond length and bond angles changes, which depends upon relaxation energies. Reorganization energy λhole and λelectron is decreasing from benzene to nonacene and rate of charge transfer increases as from electron transfer equation. These molecules can be used as organic semiconductors in optoelectronic devices, due to low λ values.These reorganization energy is related with Diffusion coefficient and distance between pair of molecules. The theoretical values of the reorganization energies are in agreement with values obtained experimentally. It is observed that Reorganization energy is according to the Franck-Condon principle. The reorganization energy (λ_{hole}) and ($\lambda_{electron}$) of cation and anion of the molecule in groundstate and in excited state are calculated, as from the Franck-Codon principle.[2,3] This property is an important parameter for determining mobility property of organic semiconductors(λ values).
The reorganization energy includes inner component factor and an outer component factor Reorganization energies are

ISSN (Online) 2456 -1304

International Journal of Science, Engineering and Management (IJSEM)
Vol 6, Issue 10, October 2021

calculated as

$$\lambda_{hole(electron)} = (E^*_{cation(anion)} - E) + (E^*_{+(-)} - E_{+(-)})$$

where E describes energy of optimization of neutral molecule, $E_{+(-)}$ explains energy of optimization of cationic or anionic molecule , $E^*_{cation(anion)}$ describes energy of neutral molecule in cationic or anionic geometry, $E^*_{+(-)}$ describes energy of cationic or anionic molecule in neutral geometry . This equation explains cationic and anionic energy in Hartrees and energy of neutral molecule. The reorganization energies were calculated at B3LYP functional and 6-31+G(d,p) basis set in Gaussian09. From rate of electron transfer equation, λ depends on nuclear wavefunctions and overlapping of wavefunctions occur which makes rate of electron transfer in these Oligoacenes. Using B3LYP functional and 6-31+G(d,p) basis set , λ has been shown to give values decreasing from benzene to nonacene.

Molecules for Reorganization Energy(eV) are determined.	**λ_{hole}(eV)**	**$\lambda_{electron}$(eV)**
PTCDA	0.144	0.251
PTCDA(N-CH_3)	0.157	0.259

In the above examples Perylene - 3,4,9,10 tetracarboxylic - 3,4,9,10 dianhydride(PTCDA) and its N-methylated analogues , the hole reorganization energy is less than electron reorganization energy. These molecules can act as high mobility organic semiconductors,due to low λ values, where π-π stacking, planarity, molecular layers add to high mobility.

Oligoacenes with good reorganization energy values are used as good organic semiconductors . Pentacene to nonacene show a sharp decrease in reorganization energy values. When λ decreases, rate of charge transfer W increases, as seen in the Marcus Equation.

$$W=\frac{2Hmn2}{h}\sqrt{\frac{\pi 3}{\lambda KBT}}\, e^{-\lambda/4KBT}$$

where H_{mn} ,is coupling matrix element(electronic coupling) between pair (m,n) of molecules, λ is Reorganization energy and K_B is Boltzmann constant. When W increases ,Diffusion coefficient(D) will increase and mobility will increase. Thus these oligoacenes from pentacene to nonacene act as High mobility good organic semiconductors in optoelectronic devices [5] .Other factors which depends on Reorganization energy are Intermolecular coupling and Transfer Integral[8,9]. Thus these reorganization energy are based on these factors also. Reorganization energy is energy required for reactants to convert to products as seen in Gibbs energy diagram with displacement coordinate. λ is reorganization energy required to convert reactant molecules to product complex, where it is utilized or used for structural rearrangement of reactant molecules and its relative orientation. These molecular rearrangements include relative reorientation of reactant molecules and relative reorientation of solvent molecules. Electron transfer can occur only after thermal fluctuations bring geometry of reactant molecules to the point, where electron transfer takes place according to Franck Codon principle.[6,7]. Rate of electron transfer in these molecules depends upon λ, which is reorganization energy and H_{mn} which is coupling matrix element between pair of molecules. H_{mn} depends upon wavefunctions of two charge localised states φm and φn between molecular pairs,which makes strength of interactions in these molecules[10].

Figure showing reorganization energies of optimized structures of Pentacene in cationic and anionic geometry using B3LYP functional and 6-31+G(d,p) basis set.

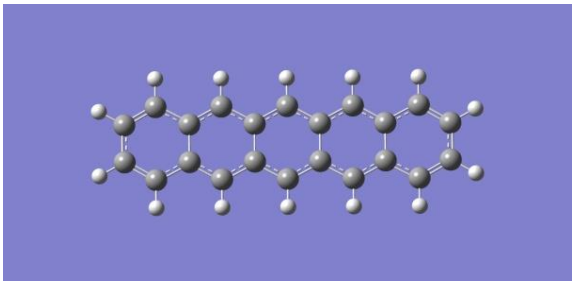

Energy of optimization of neutral molecule

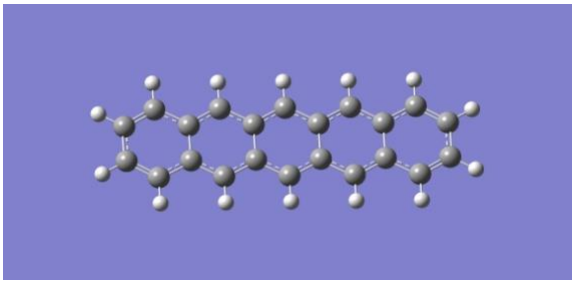

Energy of cationic charged molecule in neutral structure

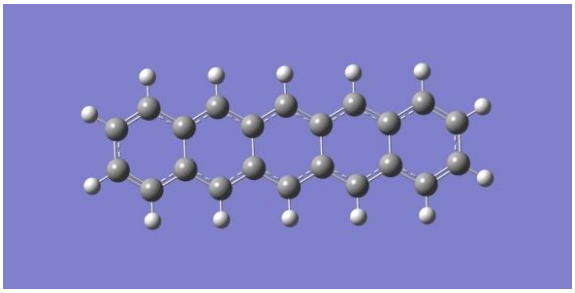

Energy of Optimized structure of cationic molecule

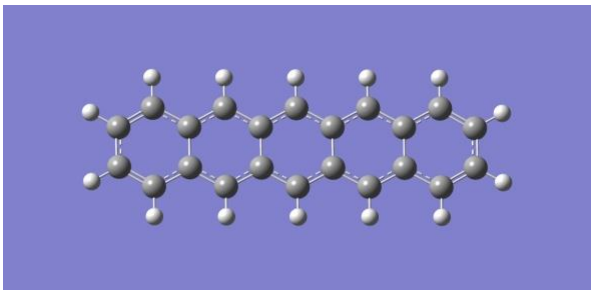

Energy of neutral molecule in cationic structure

III. SUMMARY

The development and analysis of charge carrier mobility and its electronic properties can be possible in any general computational technique like DFT. Calculation of electron and hole Reorganization energies is an important method for determining mobility and hence electronic properties of organic molecular solids. Oligoacenes with low reorganization energy values can act as high efficiency Organic Semiconductors for Organic Field effect Transisitors and has applications in hole transporting materials and electron transporting materials. These low reorganization energy values has applications in Designing of molecules and biological materials.

REFERENCES

[1] Yang, X.; Wang, L.; Wang, C.; Long, W.; Shuai, Z. Chem. Mater. 20, 3205-3211. (2008).
[2] Marcus, R. A. Rev. Mod. Phys. 65, 599-610.(1993).
[3] Marcus, R. A. J. Chem. Phys. 24, 966-978(1956)
[4] Mas-Torrent, M.; Durkut, M.; Hadley, P.; Ribas, X.; Rovira, C. J. Am.Chem . Soc., 126, 984-985(2004).
[5] Bredas, J. L.; Calbert, J. P.; daSilvaFilho, D. A.; Cornil, J. PNAS 99, 5804- 5809.(2002).
[6] Hutchinson, G. R.; Ratner, M. A.; Marks, T. J.. Hopping J. Am. Chem. Soc., 127, 2339-2350 (2005) .
[7] Hutchinson, G. R.; Ratner, M. A.; Marks, T. J. J. Am. Chem. Soc., 127, 16866-16881 (2005).
[8] Lin, B. C.; Cheng, C. P.; You, Z. Q.; Hsu, C. P. J. Am. Chem. Soc. 127, 66-67.(2005)
[9] Senthilkumar, K.; Grozema, F. C.; Bickelhaupt, F. M.; Siebbels, L. D. A. J. Chem. Phys. 119, 9809-9817.(2003).
[10] Senthilkumar, K.; Grozema, F. C.; Guerra, C. F.; Bickelhaupt, F. M.; Lewis, F. D.; Ratner, M. A.; Siebbeles, L.D.A. J. Am. Chem. Soc127, 14894-14903(2005).

Materials Today: Proceedings xxx (xxxx) xxx

Contents lists available at ScienceDirect

Materials Today: Proceedings

journal homepage: www.elsevier.com/locate/matpr

Structures of cation doped polyacenes and its binding energies across polyacene surface

Sharon Achamma Abraham Abraham *

Department of Chemistry, Mar Thoma College, Tiruvalla 689103, India

ARTICLE INFO

Article history:
Available online xxxx

Keywords:
Binding energy
Functional
Transition State Structure
Potential Energy Surface
Cation-π complex
Polyacene
basis set
B3LYP
coupling matrix element
Mulliken charge
spin transport property

ABSTRACT

The Binding energies of cation-π complexes are calculated computationally using DFT method and the B3LYP functional. The binding energies in kcal/mol using B3LYP functional and 6–31 + G(d,p) basis set in Gaussian09 has provided a source to design one-dimensional materials and to study hopping of charges in one-dimensional materials.

The Mulliken charges and ΔE in kcal/mol with bsse corrections are confirmed using B3LYP functional and 6–31 + G(d,p) basis set in Gaussian09. Above benzene ring, a cation is located at a distance of 2.5 Angstrom units above plane of molecule and binding energy ΔE)is calculated using B3LYP functional and 6–31 + G(d,p) basis set, which shows difference between energy of [benzene. . ..Metal ion complex] and sum of energy of [benzene] and [cation M^+]. Binding energies of cation-π complexes on polyacenes are determined and studied hopping dynamics. Binding energies as well as hopping energies for cations to polyaromatic hydrocarbons follows the order Li^+>Na^+>K^+. Binding energies (ΔE) decreases with size of cation(M^+) as Li^+>Na^+>K^+. When binding energy (ΔE *or* ΔG) decreases, in cation-π complexes, reaction rate k increases. This study has applications in computing rate of the reactions and in thermodynamic properties of chemical reactions.

Selection and peer-review under responsibility of the scientific committee of the International Chemical Engineering Conference 2021 (100 Glorious Years of Chemical Engineering & Technology).

1. Objective

This theoretical research work urges computational modelling and designing of oligoacenes or polyacenes in the field of semiconductors and to reveal nature of interactions. The work aims not only in improving performance of organic materials for possible incorporation in devices, but also for satisfying the need for insight into relevant physical processes that govern electrical conduction in these materials and complexes. The main objective of this work is to tune oligoacenes or polyacenes as high mobility semiconductors in the field of optoelectronic devices and to calculate parameters that enhance mobility of these polyacenes.

1.1. Methodology

The Binding energy calculations based on density functional theory(DFT) method were performed on a series of polyacenes with both one dimension(linear polyacenes) and in two-dimensions(bent polyacenes).

All ΔE energies in kcal/mol were produced using B3LYP functional and 6–31 + G(d,p) basis set in Gaussian09 [1]. B3LYP functional and 6–31 + G(d,p) polarized basis set was used[2]. All frequency calculations for transition state structures were computed in this method. The role of dispersion interactions[3] in stabilization of ground state structures were assessed by calculations at M05-2X functional and 6–31 + G(d,p) basis set.[4,5,6]

The Binding energies in kcal/mol in acene metal ion structures were performed to find lowest energy structure and to find transition state of structures. Calculations were performed for binding of Li^+, Na^+ and K^+ with various rings. The rings on edges and center are represented as S_o and C respectively. The intermediate rings are sequentially labelled as S_1, S_2, S_3 etc. starting from extreme edge(S_0). For each of the configurations, binding energies are calculated. The minimum energy configuration for cation on the ring corresponds to its location at its centre while transition states correspond to cations placed vertically over C-C bonds.

* Corresponding author.
E-mail address: sharon.1384@gmail.com

https://doi.org/10.1016/j.matpr.2022.01.117

Selection and peer-review under responsibility of the scientific committee of the International Chemical Engineering Conference 2021 (100 Glorious Years of Chemical Engineering & Technology).

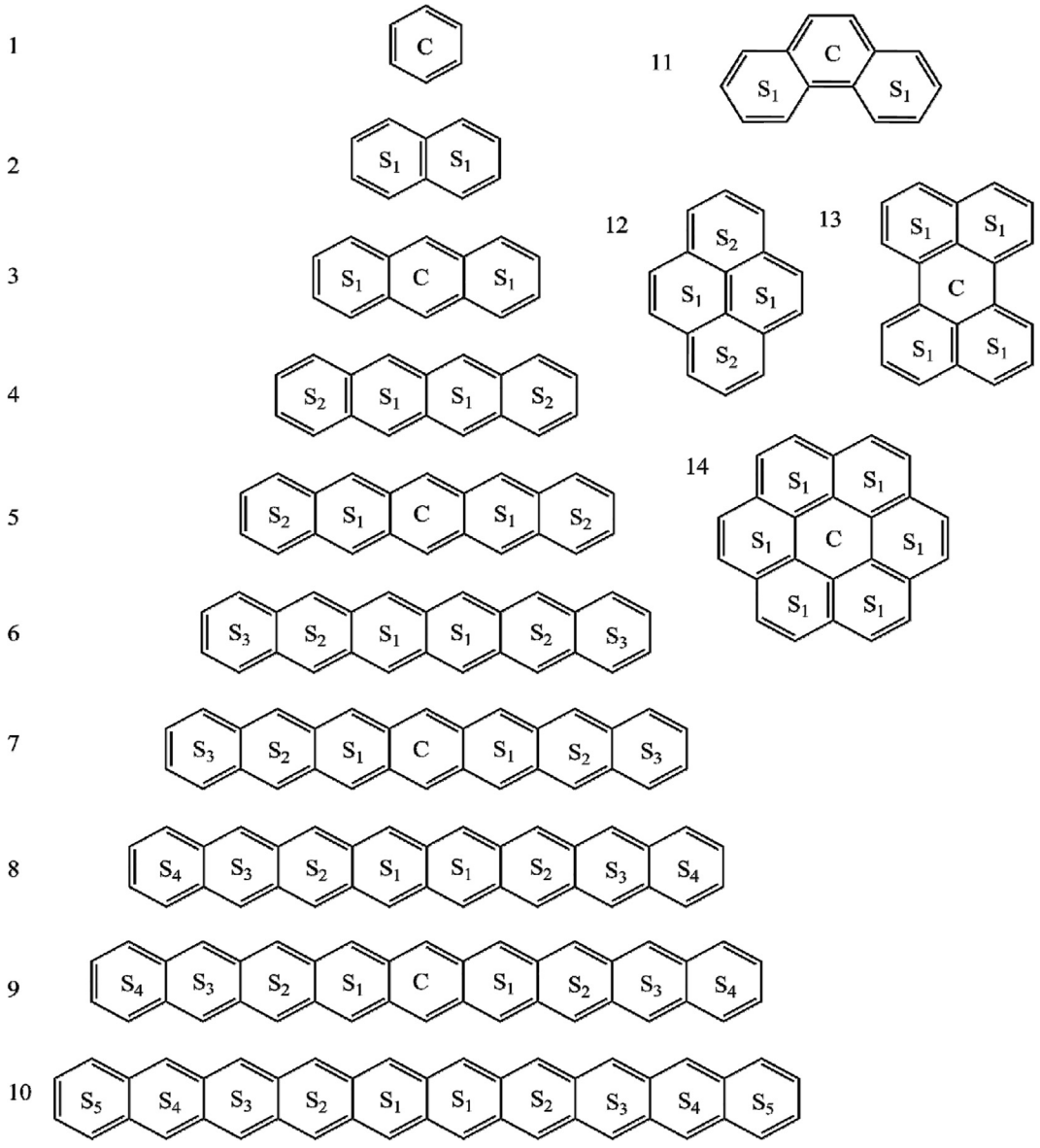

Fig. 1. Structures of acene molecules considered in Binding Energy studies.

In the table above, binding energies of cations to each of ring are calculated. For a given ring in any system, binding energies decreases with size of cation (Li^+>Na^+>K^+). Our computed binding energies[7] and trends are in good agreement with previous calculations as well as collision induced dissociation(CID) experiments for benzene.....M^+ complexes[8]. Incorporation of dispersion interactions at M05-2X functional and 6–31 + G(d,p) basis set stabilize cation...π complexes by 2 kcal/mol. Among linear polyaromatic hydrocarbons, upto tetracene, binding of cation to terminal ring is strong. This is in accordance with binding energies obtained for these systems at MP2/6-31G* level[9]. However, as number of rings increase, cation tends to bind to central ring much more effectively. The binding energies continuously decrease as we go from central ring to terminal ring.

In addition, binding energies also increase with increase in number of rings for linearly fused rings. Across the rings, binding energies for cations are large though terminal rings bind more strongly to Li^+ than central rings. In these fused acenes, terminal rings are more electron rich than central ring. The extent of charge transfer depends on distance to which cation M^+ binds to ring or aromatic π conjugated system[10]. The rate of charge transfer k, between pair of molecules(m,n) at a fixed temperature can be calculated using equation

$$k = \frac{2H_{mn}{}^2}{h}\sqrt{\frac{\pi^3}{\lambda KbT}}e^{-\Delta G/nRT} \quad \text{where } \lambda = -\Delta G$$

Hmn is coupling matrix element between pair of molecules, ΔG or ΔE is binding energy in kcal/mol, k_b is Boltzmann constant, λ is reorganization energy, $\lambda = -\Delta G$ is cancellation of reorganization energy term by standard Gibbs energy. The rate k increases, if binding energy is low and H_{mn} increases.

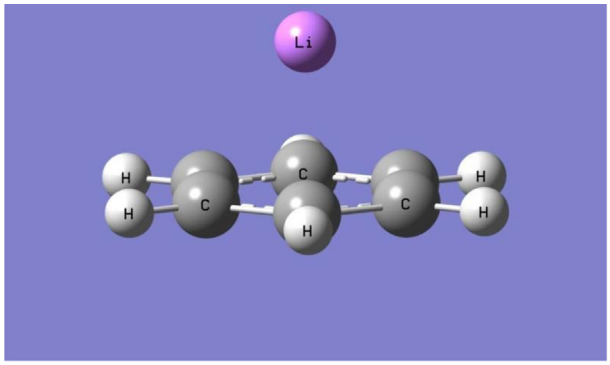

Benzene….Li^+
Distance between C and Li^+ = 2.35A°

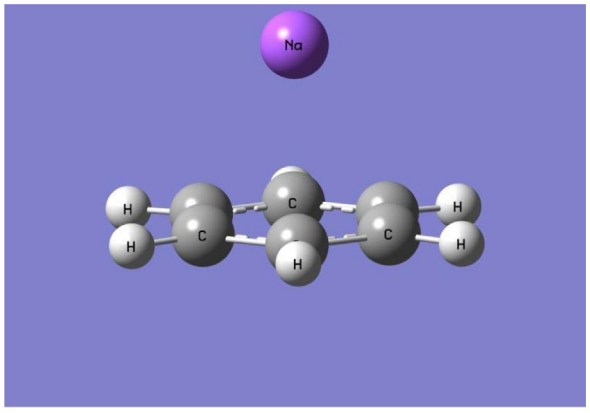

Benzene…Na^+
Distance between C and Na^+ = 2.77A°

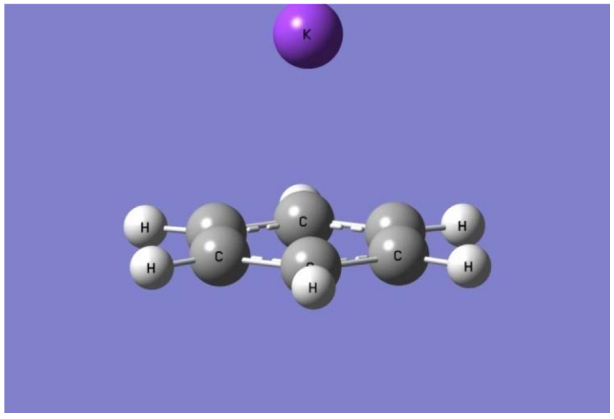

Benzene…K^+

Distance between C and K^+ = 2.77A°

Fig. 2. Structures of benzene metal ion complexes using B3LYPfunctional and 6–31 + G(d,p) basis set.

1.2. Results

Higher binding energy, is most stable of these systems. For Li^+, Na^+ and K^+, binding to Li metal is most stable. Li is the best metal selected for binding in these metal ion complexes. For Li^+ metal cation, it shows −37.24 kcal/mol, which is highest binding energy value in single aromatic ring benzene systems. For bsse corrections, it shows a value of −36.2 kcal/mol[7]. In Li^+ metal cation, binding energy value is most stable than bsse corrected binding energy value. For Na^+ metal cation, it shows a binding energy value of −24.06 kcal/mol and K^+ metal binding with single ring, it shows a binding energy value of −15.23 kcal/mol. For a single ring system, for Li^+,Na^+ and K^+ with benzene ring, binding energies are very high and most stable than bsse corrected binding energy values.

In Benzene Li^+ complex, the Mulliken charge is +0.165475 on Li $^+$ and +0.685530 on Na^+ in Benzene. . ..Na^+ complex. In Benzene. . ..K^+ complex, it shows a Mulliken charge of +0.952516 value. The charge transfer decreases in the order K^+>Na^+>Li^+. For Naphthalene binding with Li^+, it shows a binding energy value of −39.94 kcal/mol.

The bsse corrected value is −39.3 kcal/mol which is less stable than binding energy value without bsse correction. For Naphthalene binding with Na^+ metal, it shows a binding energy value of −26.37 kcal/mol. With bsse correction it shows −25.68 kcal/mol. For Naphthalene binding with K^+, it shows a binding energy value of −17.44 kcal/mol and with bsse correction, it is −16.95 kcal/mol. For Naphthalene. . ..Li^+, Mulliken charge is +0.165475 and different charges can be studied. For Naphthalene. . .. . .Na^+, it shows a Mulliken charge of +0.682036 and in Naphthalene. . .. . .K^+ it shows a Mulliken charge of +0.949310 value. Naphthalene binding with Li^+ shows minimum energy structure which is most high value suitable for binding. Naphthalene. . .. . ..Na^+ shows high rate and rate of cation hopping is very high and increases rate of reaction k, due to Quantum tunneling. The rate is very high in Naphthalene. . .. . ..Na^+ complexes due to Quantum tunneling because of smaller barrier height[12].

On plotting number of rings of fused acenes along × axis and Binding energies in kcal/mol along y axis, it is observed that Binding energies increases with number of rings of fused acenes. Binding energy is maximum for hexacene showing a value of −46.42 kcal/mol and minimum for benzene and it increases with number of rings of polyacenes.

In Naphthalene. . .. . .Li^+ complexes, the rate is high and increases with temperature. This can be explained using Arrhenius equation. Naphthalene. . .. . ..Na^+ shows high rate due to Quantum tunneling[13] and it is independent of temperature. This studies are calculated using M05-2X functional and 6–31 + G(d,p) basis set. Naphthalene. . ..Na^+ shows high rate than Naphthalene. . ..Li^+ and this shows a marked variation than Naphthalene. . ..Li^+ complexes. Naphthalene. . .. . .Na^+ complexes and Naphthalene binding with Na^+ is the most suitable complexes that can be selected because of its high rate and it shows high value. The rate of hopping is much faster for Na^+ than Li^+ due to Quantum tunneling and has smaller barrier height. M05-2X functional is used for calculating rate of the reaction, gives high rate in Naphthalene. . .. . .. Na^+ complexes and 6–31 + G(d,p) basis set is used, which gives most accurate values. M05-2X functional is used for calculating rate of reaction here and is most significant.

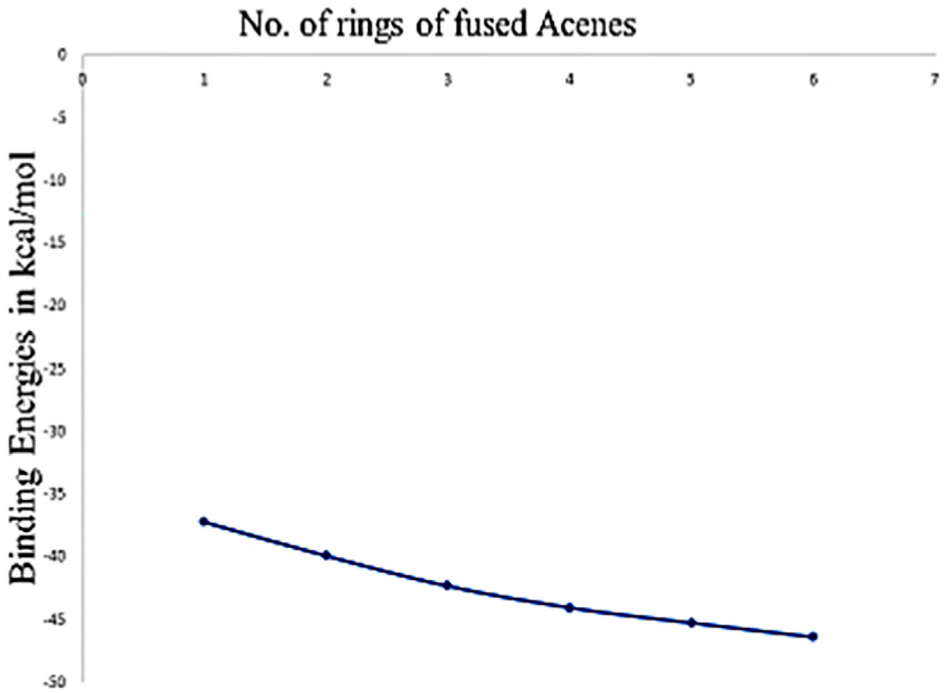

Fig. 3. Binding energies in kcal/mol as function of Number of rings of fused acenes using B3LYPfunctional and 6–31 + G(d,p) basis set.

Calculations are done in various polyaromatichydrocarbon systems from benzene to coronene (Fig. 1) using B3LYP functional and 6–31 + G(d,p) basis set. In each of system as shown in figure, a cation is located at a distance of 2.5 Angstrom units above aromatic ring and cation is moved from top of one ring (horizontally) to other end above plane of molecule. The cation Li^+, Na^+ and K^+ is moved from one end of aromatic ring to other end at a distance of 2.5 Angstrom units above plane of aromatic ring structure[10]. For each of cation Li^+,Na^+ and K^+, potential energy surface(PES) is obtained (see Figs. 2–6 and Table 1).

The hopping of cation Li^+,Na^+ and K^+ can be observed and initial structure, Transition state(TS) Structure(Intermediate Structure), and final structure can be studied. The potential energy surface for each of cation is different and hopping barriers can be observed. The cation Li^+,Na^+ and K^+ can be located at each of above ring and in the centre and binding energy is calculated for each of ring(ΔE). When binding energy ΔE *or* ΔG in kcal/mol decreases, in acene metal ion structures, rate of reaction k increases[11]. A cation Li^+, Na^+ and K^+ is placed at centre of ring in each fused acene systems and ground state structure energy in kcal/mol can be calculated. Then the same cation Li^+, Na^+ and K^+ is placed at a distance of 2.5 Angstrom units above each ring of fused acene system and binding energy in each of ring in kcal/mol can be calculated. Difference in energy between these two structures gives barrier height in these complexes.

On plotting no. of rings as first, second, third ring of fused acene along x axis and E^0 Volts Reduction potentials along y axis, it is observed that Li metal is most binding for fused acenes. Li metal is binding with fused acenes and is having a E° value of −3.05 V. $Na^+$and $K^+$is less binding than Li^+.

1.3. Significance outcome of the research study

It has applications in spin transport properties in oligoacenes. As size of conjugated ring systems increase, contribution from orbitals of atoms of edge-states decrease to overall VB resonance structure. Hence in principle, edge atoms may no longer be in conjugation with each other. Therefore for polyaromatic linearly fused rings, edge atoms might be disjoint from each other. This is shown in figure. The atoms marked red on side of chain are not correlated with their analogues on other side of chain.

For such systems, ground state can hardly be described by a single-determinant closed shell configuration. Hence, longer chain

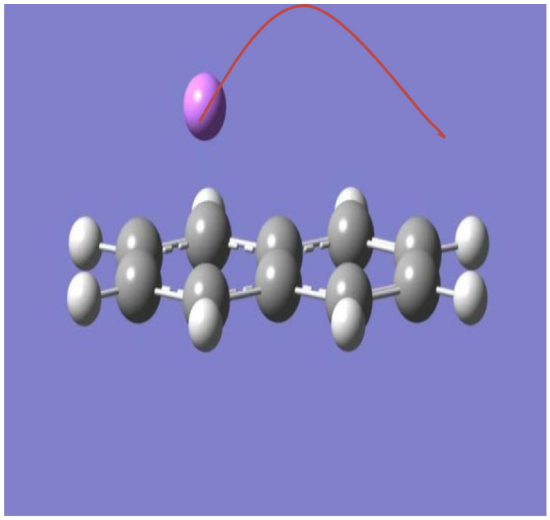

Naphthalene…….Li^+

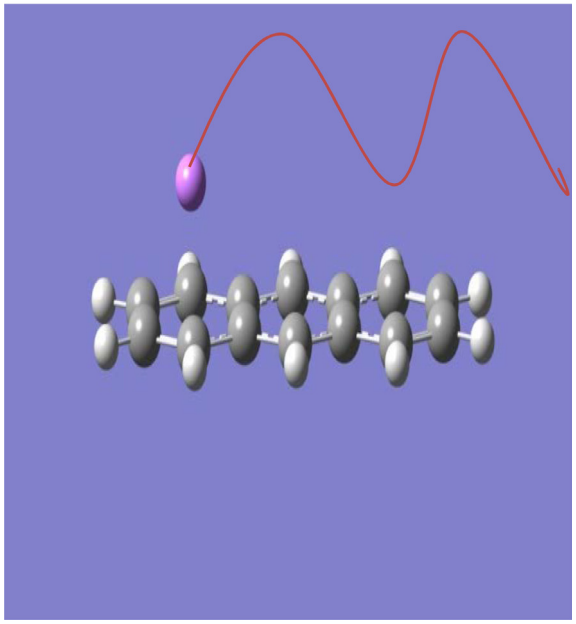

Anthracene……Li^+

Fig. 4. Structures of cation doped polyacenes using B3LYP functional and 6–31 + G (d,p) basis set.

polyaromatic hydrocarbons represent a unique class of molecular systems which can have low singlet–triplet gaps and hence can be wonderful molecules for realizing superconductivity from organic molecules. One of most important characteristic feature is its singlet triplet instability of polyacenes and electronic properties can thus be explained.

One of most important application is in fascinating properties of graphene. Graphene, a one-atom thick two dimensional layer of carbon atoms in an sp^2 bonding environment. Graphene is composed of fused benzene rings in a two dimensional arrangement exhibits transport, optical and storage properties. Graphene, due to highly mobile π electrons are polarized by presence of ions like Li^+ and this has resulted in fabrication of Lithium ion batteries(LIB) for electrochemical energy storage applications. Lithium ions(Li^+) get intercalated between graphene layers through a sandwich like complex formation with benzene rings on top and bottom. These studies has applications in mobility of cations over aromatic ring. The incorporation of hexagonal sheets of planar graphene layers, binding with cations Li^+, Na^+ and K^+ and π electron clouds, structural arrangement are very interesting and mobility of cations can be studied. The binding energy calculation with metal ions is applied in these areas. Alkali metal ions π surface can be used to design molecular structures and design of molecular materials. At room temperature, mechanism for ionic diffusion is distinctly different for Li^+ and Na^+ metal ions.

Li^+ diffuses according to Arrhenius equation, while Na^+ diffuses entirely via quantum tunneling across barrier from lowest vibrational ground state. Alkali metal ions are rather free to diffuse across aromatic surfaces of layer materials like graphene. One of most important research study is in solid state chemistry and solid-state graphene battery, band structure and band like transport behaviour of solids and in designing one-dimensional materials[14]. The band method and Fermi level can be studied. These studies has applications in interactions between aromatic rings and Li^+ cation, which are considered as cation- π interactions, between out of plane negatively charged π electrons of aromatic ring and positively charged cations. Since cations are adsorbed over π surface by weak intermolecular forces, they are expected to be highly mobile towards lateral movement across rings in graphene. This study can describe thermodynamic properties of chemical reactions and methods in electrochemistry[15]. This research study can synthesize charged molecules, and has applications in protein ligand interactions, folding of proteins and is helpful in protein studies.

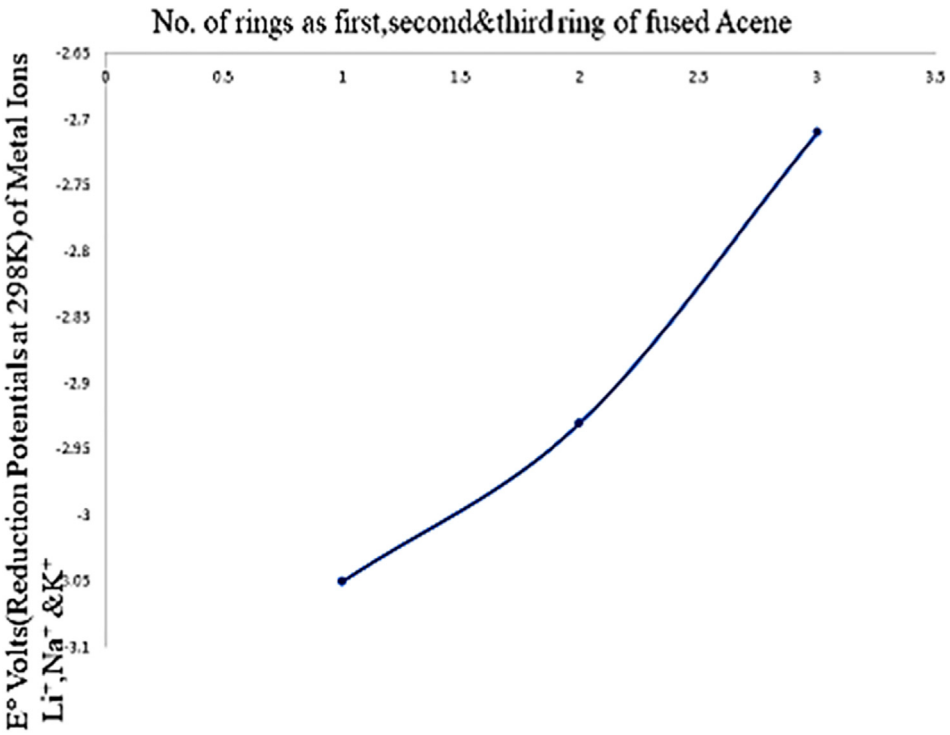

Fig. 5. E^0 Volts (Reduction Potentials at 298 K) of Li^+, Na^+ and K^+ as a function of No. of rings as first, second and third ring of fused acene.

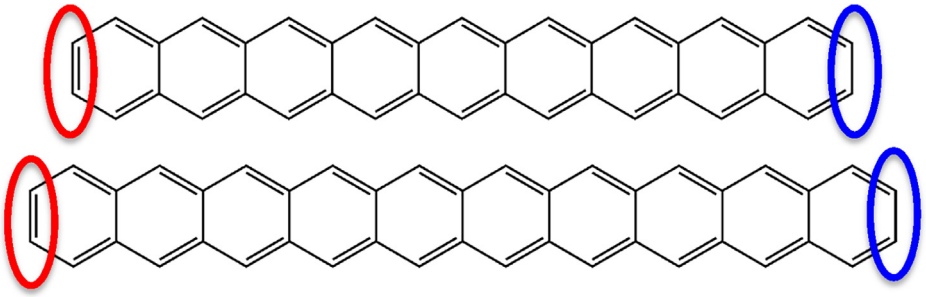

Fig. 6. Nature of disjoint edge atoms in long chain polyaromatic hydrocarbons.

Table 1
Binding Energies ΔG[a] in kcal/mol of Li^+,Na^+ and K^+ to various rings in polyaromatic hydrocarbons.

b	Metal ion	C	S1	S2	S3	S4	S5
1	Li^+	−37.24(−36.2)					
	Na^+	−24.06(−23.62)	–	–	–	–	–
	K^+	−15.23(−14.92)					
2	Li^+		−39.94(−39.3)				
	Na^+		−26.37(−25.68)				
	K^+		−17.44(−16.95)				
3	Li^+	−42.35(−41.7)	−41.63(−40.87)				
	Na^+	−28.44(−27.58)	−27.93(−27.02)				
	K^+	−18.94(−18.42)	−19.09(−18.41)				
4	Li^+		−44.08(−43.4)	−43.50(−42.77)			
	Na^+		−29.86(−29.49)	−28.98(−28.53)			
	K^+		−20.12(−19.55)	−20.26(−19.60)			
5	Li^+	−45.29(−44.59)	−44.93(−44.59)	−45.29(−44.59)			
	Na^+	−30.88(−29.94)	−30.68(−29.61)	−30.82(−29.76)			
	K^+	−20.10(−20.37)	−21.23(−20.56)	−21.33(−20.64)			
6	Li^+		−46.10(−45.42)	−46.00(−45.24)	−46.42(45.64)		
	Na^+		−31.60(−30.67)	−31.64(−30.59)	−31.89(−30.84)		
	K^+		−21.59(−20.95)	−22.00(−21.31)	−22.2(−20.95)		
7	Li^+	−46.70(−46.02)	−46.72(−45.76)	−47.32(−45.96)			
	Na^+	−32.09(−31.14)	−32.21(−31.19)	−32.66(−31.61)			
	K^+	−21.96(−21.25)	−22.85(−21.79)	−23.04(−22.14)			
8	Li^+		−47.09(−46.41)	−47.24(−46.47)	−47.96(−47.18)	−48.36(−47.6)	
	Na^+		−32.43(−31.49)	−32.66(−31.60)	−33.22(−32.15)	−−33.53(−30.69)	
	K^+		−22.26(−21.65)	−−22.26(−22.17)	−−23.33(−22.60)	−−23.59(−22.86)	
9	Li^+	−51.94(−53.93)	−51.74(−53.73)	−51.15(−53.14)	−50.28(−52.31)	−50.10(−52.29)	
	Na^+	−36.12(−38.07)	−35.96(−37.91)	−35.48(−37.43)	−34.79(−36.78)	−34.52(−36.53)	
	K^+	−24.62(−26.53)	−24.49(−26.40)	−24.10(−26.01)	−23.51(−25.43)	−22.93(−24.96)	
10	Li^+		−54.50(−54.40)	−52.16(−54.14)	−51.19(−53.68)	−50.52(−52.56)	−50.29(−52.48)
	Na^+		−36.60(−38.07)	−36.31(−37.90)	−35.77(−37.43)	−35.13(−36.78)	−34.81(−36.53)
	K^+		−25.03(−26.53)	−23.07(−26.40)	−24.33(−26.24)	−24.79(−25.60)	−23.69(−25.09)
11	Li^+	−41.12(−40.41)	−41.86(−42.52)				
	Na^+	−27.06(−27.92)	−27.69(−28.29)				
	K^+	−18.52(−19.16)	−18.33(−18.88)				
12	Li^+			−40.53(−41.27)	−42.73(−43.43)		
	Na^+			−27.19(−28.18)	−28.17(−29.08)		
	K^+			−18.58(−19.23)	−18.99(−19.59)		
13	Li^+	−40.49(−41.29)	−44.11(−44.83)				
	Na^+	−28.24(−29.37)	−29.26(−30.32)				
	K^+	−19.88(−20.63)	−19.91(−20.58)				
14	Li^+	−42.31(−41.47)	−43.95(−44.61)				
	Na^+	−28.39(−29.60)	−29.46(−30.54)				
	K^+	−20.04(−20.82)	−20.29(−20.97)				

[a] Binding Energy with BSSE correction.
[b] Refer Fig. 1.

Declaration of Competing Interest

The authors declare that they have no known competing financial interests or personal relationships that could have appeared to influence the work reported in this paper.

References

[1] (a) A.D. Becke, J. Chem. Phys. 98 (1993) 5648;
(b) C. Lee, W. Yang, R.G. Parr, Phys. Rev. B 37 (1988) 78.
[2] P.C. Hariharan, J.A. Pople, Theor. Chim. Acta 28 (1973) 213.
[3] (a) Y. Zhao, N.E. Schultz, D.G. Truhlar, J. Chem. Theory Comput. 2 (2006) 364;
(b) Y. Zhao, D.G. Truhlar, Theor. Chem. Acc. 120 (2008) 215;
(c) A.K. Jissy, U.P.M. Ashik, A. Datta, J. Phys. Chem. C 115 (2011) 12530.
[4] D.G. Truhlar, B.C. Garrett, Annu. Rev. Phys. Chem. 35 (1984) 15.
[5] , Reviews in Computational Chemistry vol. 23 (2007) 125–232.
[6] J. Zheng, S. Zhang, J.C. Corchado, Y.-Y. Chuang, E.L. Coitino, B.A. Ellingson, D.G. Truhlar, POLYRATE version. A; (2010), University of Minnesota, Minneapolis, MN, 2009.
[7] D. Umadevi, Sastry N, S. J. Phys. Chem. C 115 (2011) 9656.
[8] E. Lopez, J.M. Lucas, J. de Andres, M. Alberti, J.M. Bofill, D. Bassi, A. Aguilar, The experimental binding energies for the mono-ion adducts of lithium, sodium and potassium ion with benzene are 38.5 kcal/mol, 21.9 kcal/mol and 17.5 kcal/mol respectively, Phys. Chem. Chem. Phys. 13 (2011) 15977.
[9] D. Vijay, G.N. Sastry, Phys. Chem. Chem. Phys. 10 (2008) 582.
[10] M. Mantina, A.C. Chamberlin, R. Valero, C.J. Cramer, D.G. Truhlar, J. Phys. Chem. A 113 (2009) 5806.
[11] (a) A. Datta, D.A. Hrovat, W.T. Borden, J. Am. Chem. Soc. 130 (2008) 6684. (b) X. Zhang, A. Datta, D.A. Hrovat, W.T. Borden, J. Am. Chem. Soc. 131 (2009) 16002. (c) O.M. Gonzalez-James, X. Zhang, A. Datta, D.A. Hrovat, W.T. Borden, D.A. Singleton, J. Am. Chem. Soc. 132 (2010) 12548.
[12] Direct dynamical calculations for the reaction rates are extremely computationally expensive and are tractable only for the naphthalene... Li+/Na+ complexes Nevertheless, since the barrier heights as well as the binding energies do not vary by more than 1kcal/mol between the various size of PAH considered (1 – 14), our conclusions are well valid for the general fused aromatic systems like graphene.
[13] R.P. Bell, The Tunneling Effect in Chemistry, Chapman and Hall, London and New York, 1980.
[14] R. Kutner, Phys. Lett. A 81 (1981) 239.
[15] (a) D. Morgan, A. Van der Van, G. Ceder, Electrochem Solid State Lett. 7 (2004) A30;
(b) M.S. Islam, D.J. Driscoll, C.A.J. Fisher, P.R. Slater, Chem Mater. 17 (2005) 5085.

Ann Mary Raju

Book Chapters

- Contributed a **chapter** titled "**Distortion of Conventions in the Post- Truth Era: An Altered Perception of the Native American Identity"** for the Book *Journey Across Cultures: Literary Reflections* published by ESN Publications in January 2021. **ISBN : 978-81-950305-6-9. Pgs – 15-21**

  The book won the **India Book of Records** and **Asia Book of Records** for 'Maximum Authors Contributing for A Book on Covid - 19 and its Impact'. The book also won the **World Book of Records** for the 'Thickest Book in the World'

- Contributed a **chapter** titled **Said and unsaid: A Glimpse into the Cultural Appropriation of Native Americans** for the Book ***Since History Begun: Unveiling the Life of the Indigenous People***.

  ISBN: 978-93-91314-42-2

Contributed a chapter titled “Spatial Aesthetics: A Post-Truth Reading of T.S. Eliot’s “Hippopotamus” for the Book *Latest Innovation for Future Education* published by ESN Publications in January 2021